Chemical Engineering Journal 505 (2025) 159146

Contents lists available at ScienceDirect

Chemical Engineering Journal

journal homepage: www.elsevier.com/locate/cej

Opposite effect of the Cu photodeposition on the •OH generation and diclofenac degradation depends on the exposed anatase facet

Szymon Dudziak [a,*], Jakub Smoliński [a], Adam Ostrowski [b], Aleksandra Szkudlarek [c], Mateusz Marzec [c], Krystian Sokołowski [c], Karol Sikora [d], Anna Zielińska-Jurek [a]

[a] Department of Process Engineering and Chemical Technology, Gdańsk University of Technology, G. Narutowicza Street 11/12, 80-233 Gdańsk, Poland
[b] Institute of Molecular Physics, Polish Academy of Sciences, M. Smoluchowskiego 17, 60-179 Poznań, Poland
[c] Academic Centre for Materials and Nanotechnology, AGH University of Krakow, Av. Mickiewicza 30, 30-059 Krakow, Poland
[d] Department of Inorganic Chemistry, Faculty of Pharmacy, Medical University of Gdańsk, M. Skłodowskiej-Curie 3a Street, 80-210 Gdańsk, Poland

ARTICLE INFO

Keywords:
Crystal facets
Cu photodeposition
Diclofenac
Degradation pathway
Z-scheme

ABSTRACT

Exposition of a specific crystal facets and modification with co-catalysts are often used in order to improve photocatalytic activity of a material. However, considering complexity of these interactions, it is still challenging to fully understand and predict activity of a specific system. Here, we report combination of the {0 0 1} and {1 0 1} crystal facets of anatase TiO_2 with Cu_XO co-catalyst, applied for diclofenac degradation, •OH generation and 4-nitrophenol reduction. Interestingly, we observed opposite effect of Cu for •OH generation and DCF degradation, with clear enhancement of the activity observed only for the {0 0 1} facets. EPR measurements further proved that for the most active material in this series, Cu exist as an atomically-scattered Cu^{2+} species at the surface, achieved as the result of high surface development and high adsorption energy (from DFT). Based on the absorbance measurements and XPS analysis, these species are shown to be further reduced to Cu_2O during degradation process. Compared to this, all other systems ({1 0 1} and all results for nitrophenol) showed reduction of the activity due to the Cu_XO presence. In this regard, Cu_XO cannot be seen as an universal reduction co-catalyst for TiO_2, with final effect being clearly dependent on exposed facet and reaction. This is despite TiO_2/Cu_XO was found to form analogical, well-known Z-scheme junction in case of both surfaces. Ultimately, we showed that specifically {0 0 1} with Cu_XO make highly synergistic combination for ROS generation.

1. Introduction

Photocatalytic degradation of organic pollutants is a promising strategy for enrironemntal remediation, which ideally does not require additional energy input apart from the sunlight. During the process, photocatalyst is not consumed, and the process takes place with the participation of solar radiation. However, due to the specificity of the solar light spectrum and the fact that the most commonly used photocatalysts, with TiO_2 at the forefront, show maximum absorption in the UV range, photocatalyst design is crucial regarding efficient utilization of incident light.

In this regard, multiple approaches are presented in order to improve photocatalyst performance. For example, surface modification with noble metals such as gold (Au), platinum (Pt), or silver (Ag) are a popular way to improve photoactivity. In such systems, deposition of the metal nanoparticles on the photocatalyst surface create heterojunctions capable of increased light absorption, mostly due to the effect of surface plasmon resonance (SPR) [1]. Occurrence of the SPR on metal surface creates possibility for electron transfer into the conducting band of TiO_2, therefore increasing its photoactivity and additionally extending time of electron-hole recombination as the result of the metal–semiconductor junction (Shottky junction) [2,3]. However, using noble metals as co-catalysts increase overall cost of the materials, leading to the situation where other metal species gather increasing attention as an alternative to Au/Ag/Pt. From these possibilities, modification with copper became a promising way to increase TiO_2 activity, especially under continuous irradiation in the visible and UVA range, due to the formation of the Z-scheme junction between the TiO_2 and Cu_XO species that forms as the result of partial copper oxidation at the TiO_2 surface [4].

However, despite rather large interest in the TiO_2/Cu system in the photocatalysis, some aspects of their operation still remain unknown. Particularly, this connects with interactions between Cu and TiO_2

* Corresponding author.
E-mail address: szymon.dudziak@pg.edu.pl (S. Dudziak).

https://doi.org/10.1016/j.cej.2024.159146
Received 29 August 2024; Received in revised form 21 December 2024; Accepted 29 December 2024
Available online 30 December 2024
1385-8947/© 2025 The Authors. Published by Elsevier B.V. This is an open access article under the CC BY license (http://creativecommons.org/licenses/by/4.0/).

surface features, such as a crystal facet engineering, which lately became important topic in the photocatalyst design [5–7]. Due to the anisotropy of the electronic properties in bulk crystal, termination of its structure with different crystal facets can heavily affect final properties of the material. This includes e.g. surface work function, band positions, surface energy and density of surface undercoordinated sites, which all affect further localization of excited charge carriers and interactions with surrounding species [8,9]. In case of the anatase TiO_2, its {0 0 1} amd {1 0 1} terminations are known to possess fundamentally different electronic properties, due to the unique electronic structure of the (0 0 1) crystal plane [10]. As the consequence, electron localization is known to be hindered for the {0 0 1}, while its favored on the surface atoms of the {1 0 1}. In this regard, both these surfaces are intriguing materials for further modifications with co-catalyst. For example, theoretical predications of the {1 0 1} termination with different metal nanoclusters were made concerning H_2 generation [11]. For such application, some interest in the {0 0 1} facets could also be noted, especially after their modification with Pt [12–14]. However, since it is still challenging to predict how fundament properties (e.g. change in work function) will affect efficiency of the specific photocatalytic process, it is still needed to systematically increase our knowledge about application of crystal facets in their bare and modified form for a different photocatalytic reactions. Concerning modification of different TiO_2 crystal facets with Cu, existing results report some of the possible applications. For example, Wei et al. studied Cu modification of anatase particles with either {1 0 1} or the combination of {0 0 1} with {1 0 1} facets exposed in the reaction of acetic acid decomposition [15]. However, more complex organic compounds were not investigated, as well as information about generation of reactive species in such system is generally missing. Also, nanoparticles that would exposed majority of the {0 0 1} were not investigated.

In this regard, we have especially focused on this problem and compared interactions between photodeposited Cu and {0 0 1} or {1 0 1} crystal facets of anatase TiO_2. Modified and bare materials were studied for the degradation of diclofenac, which is one of the most frequently used non-steroidal anti-inflammatory drug (NSAID) [16,17]. Due to its popularity and ineffective treatment processes in wastewater treatment plants (3 to 60 % removal, depending on the method), it is commonly found in surface waters [18], inducing negative impact on aquatic organisms such as algae, crustaceans, and fishes [19–23]. Furthermore, generation of •OH radicals by the prepared materials was studied in detail and discussed with respect to the electronic structure of the exposed anatase facet, followed by the 4-nitrophenol reduction.

2. Experimental

Detailed experimental description can be found in SI, Section 1.

2.1. Preparation of the TiO_2

Anatase nanoparticles with either {0 0 1} or {1 0 1} facets exposed in majority were prepared solvothermally based on the previous reports [24–26]. Briefly, for the {0 0 1} exposition, titanium n-butoxide (TBT) was mixed with the ethanol and concentrated HF solution and reacted at 180 °C for 10 h (please, be cautious that HF solutions are extremely dangerous and appropriate precautions must be used during work e.g. neoprene gloves and calcium gluconate gel are recommended for hand protection and neutralization after possible skin exposure). For the dominant exposition of the {1 0 1} facets, commercial P25 was hydrothermally treated with KOH solution to obtain $K_2Ti_6O_{13}$ precursor. Obtained titanate was H-exchanged using HNO_3, washed with water and dried. Finally, $H_XK_{2-X}Ti_6O_{13}$ was transformed into octahedral TiO_2 by reacting at 210 °C for 18 h with ammonia buffer. Final products were washed, neutralized with NaOH (in case of {0 0 1}), dried and hand-grounded.

2.2. Cu photodeposition

The photodeposition process was carried out in a quartz reactor using $CuSO_4$ as the Cu source and 50 cm^3 of 50/50 v/v ethanol–water mixture as environment. The suspension was stirred and purged for 30 min with nitrogen, closed tightly and 1 h with a 300 W Xe lamp. Modified material was washed multiple times and dried.

2.3. Structural characterization

Crystal structure of the prepared samples was analyzed using powder X-ray diffraction (XRD) with the Rigaku MiniFlex diffractometer and the Cu Kα radiation source. The refinement of the pattern performed with the available.cif file of the anatase structure (COD ID 9015929). The absorption properties of the powders were analyzed using ThermoFisher Scientific Evolution 2000 spectrometer (0.5 nm resolution) with the $BaSO_4$ as a standard for the diffuse reflectance spectroscopy measurements (DR-UV/vis). For the measurements of the suspensions we have followed procedure suggested by Cabrera et al. The measurements were performed between the 300–800 nm, with the 10 nm step. Surface areas were determined from the BET adsorption isotherm of N_2 at 77 K, after degassing of the sample under N_2 flow at 200 °C for 2 h. X-ray photoelectron spectroscopy (XPS) measurements were performed using a PHI VersaProbeII Scanning XPS system with monochromatic Al Kα (1486.6 eV) X-rays All XPS spectra were charge referenced to the unfunctionalized, saturated carbon (C-C) C1s peak at 285.0 eV. Transmission electron microscope images were collected using TEM TECNAI TF 20 X-TWIN microscope by FEI, operating at 200 kV, which is equipped with field emission gun. Photoluminescence spectra were recorded using Shimadzu RF-6000 spectrofluorometer with 300 nm and the $\lambda < 400$ nm cut-off filter on the emission side.

2.4. Local volume rate of photon absorption (LVRPA) modeling

The local volume rate of photon absorption (LVRPA) distribution within the photocatalytic rector was estimated with the six-flux model (SFM [27,28]), using procedures described by Acosta-Herazo et al. [29]. Detailed procedure is described in SI.

2.5. Photocatalytic studies and analytical procedures

Evaluation of photocatalytic activity was carried out in a cylindrical reactor with a water jacket cooling, airflow and a quartz glass as the UV–vis entry. We used a 300 W xenon lamp (LOT Oriel, Darmstadt, Germany) with both IR and $\lambda < 310$ nm radiation filters as the light source. The UVA light intensity maximum on the reactor surface was adjusted as 24 $mW \bullet cm^{-2}$. DCF solution with a concentration of 20 $mg \bullet dm^{-3}$ or 500 $\mu mol \bullet dm^{-3}$ coumarin solution were used for the photocatalytic studies. Analysis of the DCF and its by-products was performed with HPLC detection (MS and DAD), while formation of 7-hydroxycoumarin was determined via its fluorescence. Estimation of errors associated with the adapted procedures was based on the repeated processes for the selected cases. The highest observed error was than adapted for the remaining experiments. Detailed results are shown in SI, section 5.

2.6. Computational details

Molecular properties of the proposed diclofenac by-products were simulated using Orca 5.0.4 software [30] with the B3LYP functional, aug-cc-PVDZ basis set and CPCM model of solvation. All structures were geometry-optimized using BFGS algorithm to the standard convergence criteria Absorption spectra were simulated using time-dependent density functional theory (TD-DFT). The energy difference between diclofenac and its byproducts was finally calculated using H_2O, O_2 and H_2 energies.

MOST WIEDZY Downloaded from mostwiedzy.pl

Interaction between TiO_2 surfaces and Cu atoms were additionally investigated using Quantum Espresso 7.2 software package [31] with PAW pseudopotentials. Energy cut-offs for wavefunction and charge density were 40 Ry and 400 Ry respectively. We used 3x3x1 and 3x2x1 slab models with a single k-point for {0 0 1} and {1 0 1}surfaces respectively however, to reduce computational cost their thickness was reduced approximately by half. Single Cu atom was introduced on each surface to study its adsorption and resulting DOS distribution.

3. Results and discussion

3.1. Structure of the unmodified TiO_2 with dominant exposition of {0 0 1} and {1 0 1} facets

Both prepared TiO_2 samples were found to be single-phase anatase powders, without other signals observed in the XRD patterns, as presented in Fig. 1a, including Rietveld refinement of the anatase crystal structure ($\chi^2 = 2.322$ for the {0 0 1} exposition and 2.332 for the {1 0 1} one). Despite this, both patterns show significant differences in the overall character. In the case of the {0 0 1} exposition, selective broadening of the signals with high values of the *l* index is clearly observed, e.g. for the (0 0 4), (1 0 5) and (1 1 6) planes, which agrees with the expected 2-dimensional character of the obtained particles [25]. Although it is known that precise determination of the crystallite size from XRD patterns is a challenging problem [32], it can be estimated that their corresponding sizes along the [0 0 1] direction are approximately 16 nm for the {0 0 1} and 400 nm for the {1 0 1}, which gives over 20 times difference between both materials. Furthermore, highly anisotropic growth of the {0 0 1} exposing sample resulted in a slight increase of the unit cell volume, compared to the {1 0 1} sample, as well as relatively lower crystallinity of the structure, which can be noticed due to lower intensity of the overall pattern. Both these observations are in logical agreement with the small crystallite size along the *l* direction for the {0 0 1} exposing sample, since it is known that perfect bulk crystal structure is commonly not conserved near the surface. In this regard, XRD characteristics confirm expected morphological differences for the {0 0 1} exposing sample.

Following crystal structure analysis, both materials were investigated spectroscopically to check their absorbance properties and chemical states at the surface. Fig. 1b presents the results of the DR-UV/vis measurements with bandgap determination using the Tauc method in the inset. As observed, both materials show absorbance spectra characteristic for anatase TiO_2, with the main electron transition between the valence and conduction band occurring at approximately 400 nm. Interestingly, compared to the {1 0 1}, the bandgap of the {0 0 1} exposing sample is slightly reduced by ~0.1 eV with the final value of 3.16 eV. This effect is contradictory to the common observations that the bandgap of different semiconductors is increasing for smaller nanostructures [33,34]. In this regard, it is noteworthy that previous reports have concluded that for the isotropic anatase nanoparticles, analogical bandgap variation with size is almost negligible [35]. On the other hand, DFT-based simulation of the (0 0 1) model has previously suggested the existence of the additional electronic states on this specific surface, which could result in the bandgap narrowing [36]. Analogical increased activity in the visible light region was also suggested for the {0 0 1} facets in the photooxidation of formic acid [37]. In this regard, smaller bandgap is expected to result from the specific structure of the {0 0 1} facets, rather than size effects or impurities. In the case of the {1 0 1} sample, the determined bandgap is in a range of commonly reported values at room temperature.

Finally, acquired high-resolution XPS spectra in the Ti 2p, O 1 s and C 1 s regions after the fitting procedure are shown in Fig. 1c. As can be seen, in both cases, Ti exists solely as the Ti^{4+} species, in accordance with the stoichiometric TiO_2 structure. Particularly, no reduction of the surface can be noticed. This is in agreement with the amount of the lattice oxygen observed in the O 1 s spectra for both samples (O-Me at approx. 530 eV), which give O/Ti ratios equal 1.99 for the {001} exposing sample and 2.13 for the {101} one, as well as the absorbance results which have not indicated any absorption increase in the NIR region [38]. Another signals observed in the O 1 s spectrum show only moderate differences between both materials and generally follow the characteristics of the C 1 s signal (that is, higher O 1 s signal ascribed to the mixed O-C and –OH species in case of the {101} sample correlates with the higher O-C signal in the C 1 s spectrum as well). Finally, in the case of the {001} sample, the signal corresponding to the adsorbed fluorine (~684 eV) was noticed with the final Ti/F ratio of

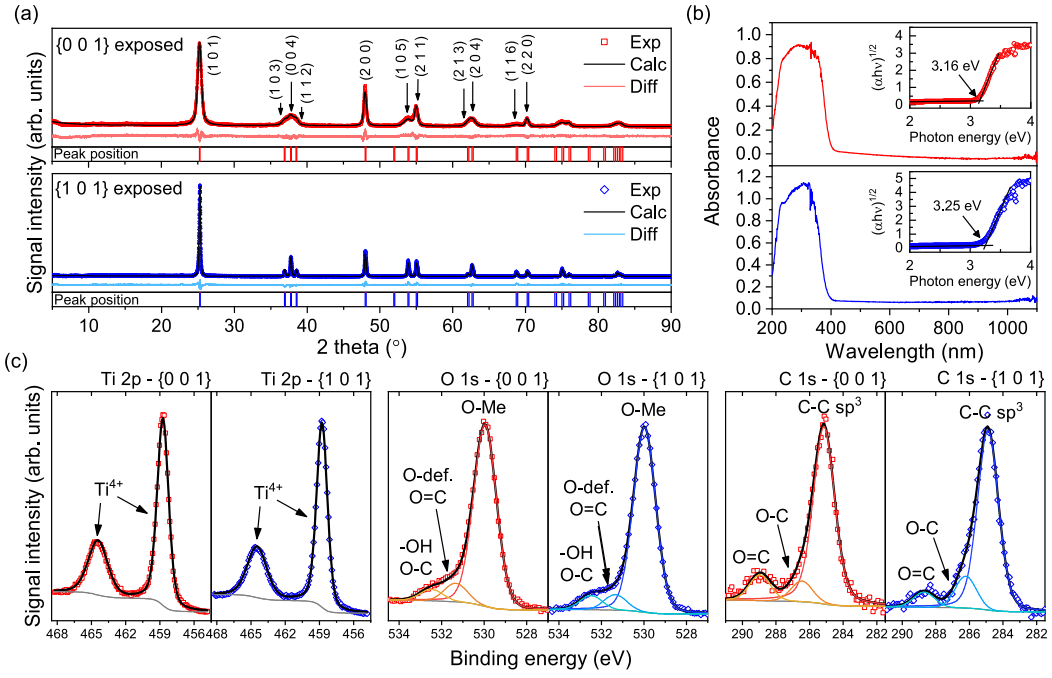

Fig. 1. Rietveld-refined XRD patterns of the prepared TiO_2 samples (a), together with the corresponding absorbance spectra (b) and deconvoluted high-resolution XPS signals for the observed elements (c). Inset of (b) presents bandgap determination using Tauc method for the indirect transition.

MOST WIEDZY Downloaded from mostwiedzy.pl

approximately 4. This is fluorine residue left after the preparation, which is commonly observed in similar materials [39,40]. Besides this, other differences result most likely from the adsorbed impurities and the oxide surface itself in both cases is almost identical before the modification with Cu.

Fig. 2 shows TEM/HRTEM images of the prepared samples. As presented in Fig. 2a, in the case of the HF-assisted synthesis, the 2-dimensional morphology of the nanoparticles is clearly observed. The HRTEM analysis of the selected plates (Fig. 2b) revealed their single-crystalline nature, as confirmed by the discrete diffraction pattern obtained from the fast Fourier transform (FFT). Moreover, despite a slightly twisted orientation of the particles, these images confirmed expected orientation of the crystal structure, with symmetrical patterns observed in both directions towards the edges of the plates, in accordance with the fourfold symmetry of the anatase unit cell along its *c* axis (visualization of the approximated orientation of a crystal structure is presented in Fig. 2b). Moreover, in the case of the {1 0 1} exposing nanoparticles, their octahedral morphology can be easily observed (Fig. 2c), in accordance with the 8 equivalent (1 0 1) planes exposed. Analogically, HR-TEM observations confirmed their single-crystalline nature, with the FFT diffraction pattern corresponding to the [1 0 0] zone axis of the anatase crystal structure when analyzing isolated octahedron from its side (Fig. 2d). Based on these results, the successful preparation of both materials was clearly confirmed. Finally, structural characterization was completed with the control measurements of the specific surface areas of both materials using the BET method. These analyses revealed the high difference in the surface development, being either 122 or 13 $m^2 \bullet g^{-1}$ for the {0 0 1} and {1 0 1}, respectively. This difference results from the adapted preparation procedures, needed to stabilize specific facet, where condensation of TBT (strictly bottom-up process) allows to achieve high surface development. On the other hand, transformation of the solid precursor used for the preparation of the {1 0 1}, P25 and K-titanate, allows only for a limited control over surface development.

3.2. LVRPA analysis and diclofenac degradation over unmodified samples

Following the large difference in the specific surface area of both materials, optical properties of their suspensions were investigated, in order to further compare their activity under similar illumination of the reaction system. Fig. 3a and b show trends of the average measured absorbance between 300–380 nm, including either the light transmitted directly through the suspension (a) or both light transmitted directly and after scattering on the particles (b). Based on the obtained data, spectral average extinction (β) and absorption (κ) coefficients were determined as the slope of these trends, with correction on the optical path in both cases (L). The difference between these values results from the light scattering on the particles. As presented, the absorption coefficient of both materials is fairly similar, however, particles with high {0 0 1} exposition show visibly higher β values, which indicate larger scattering in this system. This difference is reasonable, since it is well known that light scattering is a complex process, affected by many factors such as particle shape, size and possible agglomeration [41]. In this regard, the platelet shape of the {0 0 1}-exposing particles and different surface potential of the (0 0 1) plane might be a source of increased scattering. Following this observation, the apparent optical thickness (τ_{app}) of the utilized photoreactor was calculated for different loadings of both TiO_2 structures, as presented in Fig. 3c. Ultimately, the TiO_2 concentrations of 0.4 $g \cdot dm^{-3}$ and 0.5 $g \cdot dm^{-3}$ were selected respectively for the {0 0 1} and {1 0 1} exposing structures, which corresponds to the τ_{app} of approximately 7. Ideally, the $\tau_{app} = 1$ value corresponds to the minimum photocatalyst loading required for total absorption of the incident light and therefore should result in the most uniform irradiation of the whole reactor space. However, a very low number of dispersed particles also reduces the available surface sites for the reaction to occur. Therefore, maximum activities are commonly observed for higher τ_{app} values, which represents the compromise between a large volume of the reactor being effectively irradiated and a large number of active sites being "free" for reaction. Noteworthy, different values of τ_{app}, such as a 3–4, are often suggested as optimal for different TiO_2 materials [28,29], although, it should be noted that photocatalytic processes are known to be sensitive to the technical details of the experimental setup and in this regard, we have previously observed that reduction of the TiO_2 concentration below ~ 0.5 $g \cdot dm^{-3}$ significantly decrease final activity in our case [9]. Therefore, $\tau_{app} = 7$ was adapted for further studies. As presented in Fig. 3d, both materials show almost identical course of the LVRPA curve under such conditions. After applying detailed distribution of the UVA light that reaches the reactor border (Fig. 3e), this results in approximately 60 % of the reactor cross-section being effectively irradiated in both cases (Fig. 3f with limit adapted as the 1 % of maximum LVRPA value).

Following LVRPA analysis, the photodegradation of diclofenac (DCF) was studied under the selected photocatalyst concentrations and compared to the spontaneous photolysis (Xe lamp as the light source with an additional 310 nm filter to cut-off high energy UV radiation). As presented in Fig. 4a, photodegradation of DCF under such conditions was quite efficient, with approximately 85 % degradation observed after 60 min of irradiation. As presented in Fig. 4c, photolysis of DCF results in the formation of multiple by-products characteristic of this process, which are marked as P1-P4. Further combination of MS analysis (spectra in SI, Fig. 1 section 2), DAD spectra and molecular simulations revealed that these structures are mostly carbazole derivatives, formed due to the initial dehydrohalogenation of the DCF molecule (product P1) with subsequent hydroxylation and oxygenation of the benzene rings (P2-P4). As presented in Fig. 4d, the accumulation of these products over time shows different kinetics, supporting step-by-step transformation mechanism of these compounds. During this process, product P4 might

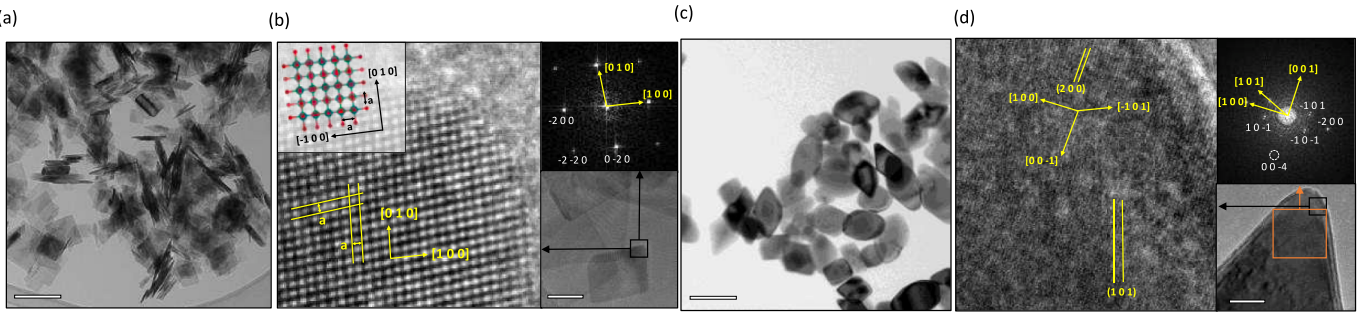

Fig. 2. Exemplary TEM images of the prepared TiO_2 samples, including nanoparticles with dominant {0 0 1} exposition (a), selected HRTEM image of the individual nanoplate (b), nanoparticles with dominant {1 0 1} exposition (c) and selected HRTEM images of the individual octahedron (d). The HRTEM images are accompanied by the FFT transformation, that corresponds to the diffraction pattern, as well as visualization of the approximated orientation of the anatase crystal structure for the {0 0 1} exposition. Scalebars are 200 nm for the panels (a) and (c); and 20 nm for the (b) and (d).

MOST WIEDZY Downloaded from mostwiedzy.pl

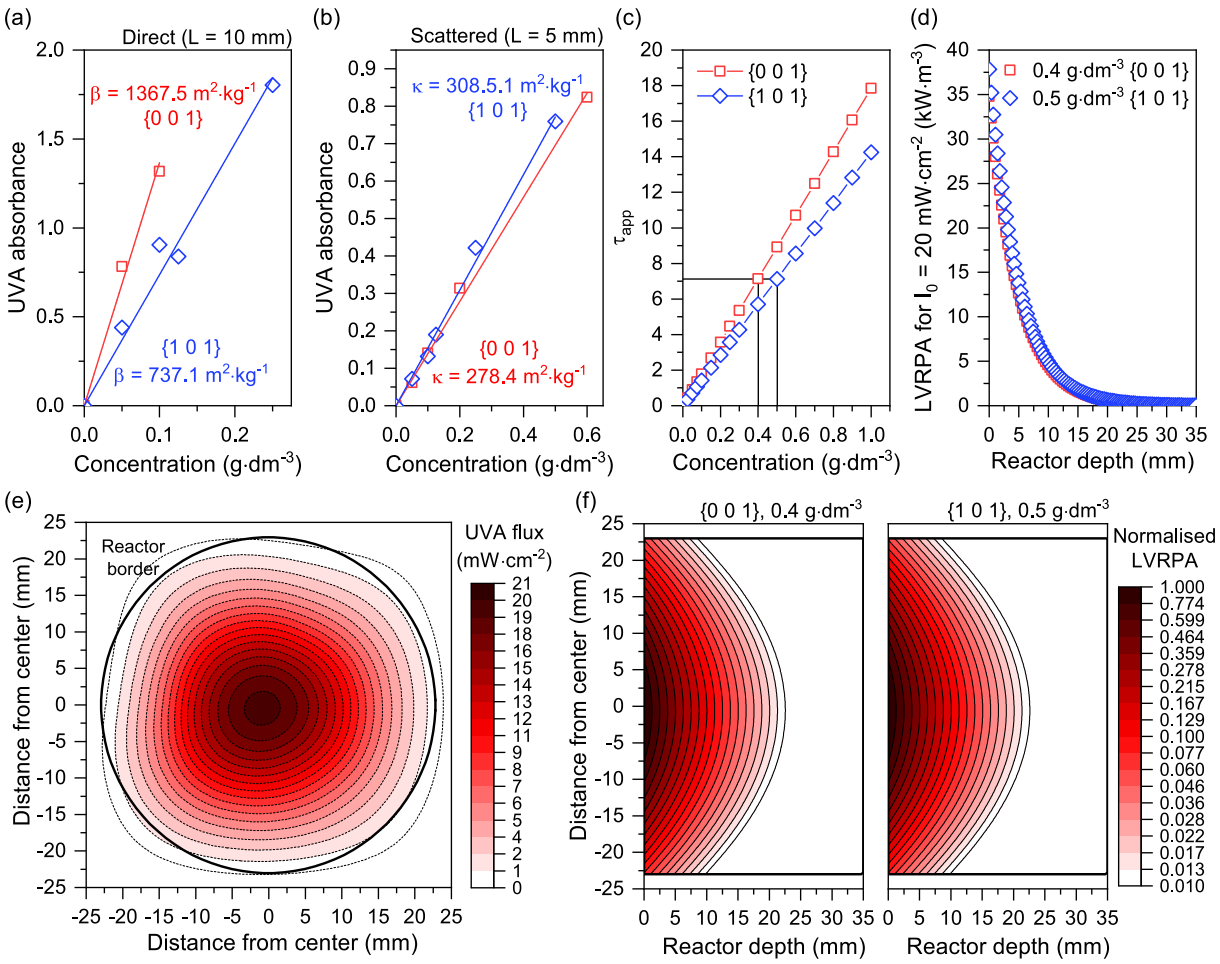

Fig. 3. Determination of spectral average extinction β (a) and absorption κ coefficients (b) of the suspensions in the light range of 300–380 nm, as the slope of the linear absorbance vs. concentration trend. The calculated apparent optical thickness τ_{app} of the suspension as the function of the photocatalyst concentration (c) and detailed LVRPA curve for the selected τ_{app} conditions at the reactor center (d). The UVA flux distribution at the border of reactor used for the photocatalytic experiments (e) and comparison of the LVRPA distribution in the full reactor cross-section for both TiO_2 materials, colored between 100–1 % of the maximum LVRPA value presented in panel d (f).

be seen as particularly interesting, due to the clear appearance of the unique ~ 420 nm absorption band. Excessive simulation of the possible structures suggests that such visible-light absorption is strictly connected with the transformation of the amine moiety (–NH-) to the imine one (=N-) within the DCF structure (Fig. 4g), which must also involve substitution of the benzene rings with keto-oxygen. Ultimately, we propose a detailed P4 structure, as presented in Fig. 4e. Noteworthy, the transformation between the P3 and P4 closely resembles this between the hydroquinone and benzoquinone, described in detail for the phenol degradation.

Compared to the simple photolysis, the introduction of the TiO_2 slightly improves overall DCF removal, however both mechanism and the kinetics of this process differ significantly. In the case of the {0 0 1} exposing structure, the adsorption during in-dark stabilization of the system achieved nearly 90 %, of initial DCF concentration, which was followed by selective formation of only one degradation by-product in the suspension (P5), as presented in Fig. 4a and 4d. Both MS data and absorption spectra clearly identify the P5 as hydroxylated DCF, without additional changes to the parent molecule. On the other hand, the {1 0 1} exposing sample shows negligible adsorption ability with a clearly improved DCF degradation after light introduction. Interestingly, in this case, both P1 and P2 products were also observed, independently of the preferred P5 formation. Ultimately, MS analysis has indicated the formation of the additional product P6 in this case, with the observed *m/z* (+) = 310.0. The possible structure of this product is presented in Fig. 4e, however it should be noted that, similarly to the P4, such structure should exhibit absorption at approx. 520 nm, which was not observed in the DAD spectra, possibly due to its low concentration. Noteworthy, as shown in Fig. 4f, DFT simulations clearly suggest that hydroxylated products (P5 and P3) are particularly stable, which might be additionally responsible for the preferred P5 formation in the TiO_2 presence. Moreover, further transformation of P5 to P6 is clearly endothermic, which also supports its possibly low concentration and absence in the DAD spectra. Optimized models of the simulated molecules are presented in Fig. S2. Finally, we will note that TOC measurements indicated increased mineralization efficiency of the TiO_2-assisted degradation than simple photolysis (approx. 40 % for the {1 0 1}, 23 % for the {0 0 1} and 1 % for photolysis). This shows that despite efficient dehydrohalogenation, UVA alone is not effective for the diclofenac mineralization which was also observed for other compounds [42]. Detailed TOC results are presented in SI (Fig. S3).

Ultimately, the effect of both TiO_2 presence and its exposed facets were clearly observed in the DCF degradation kinetics and mechanism. Particularly, significant adsorption and selective formation of P5 were observed in the case of the {0 0 1} facets. Noteworthy, both these observations are closely related. Firstly, high energy of the clean {0 0 1} facets [43] should stimulate DCF adsorption, creating a complex between undercoordinated 5c-Ti atoms and $–COO^-$ group [44–46] (please note that during the degradation in water, DCF is in its deprotonated salt form, but became protonated again during the chromatographic

MOST WIEDZY Downloaded from mostwiedzy.pl

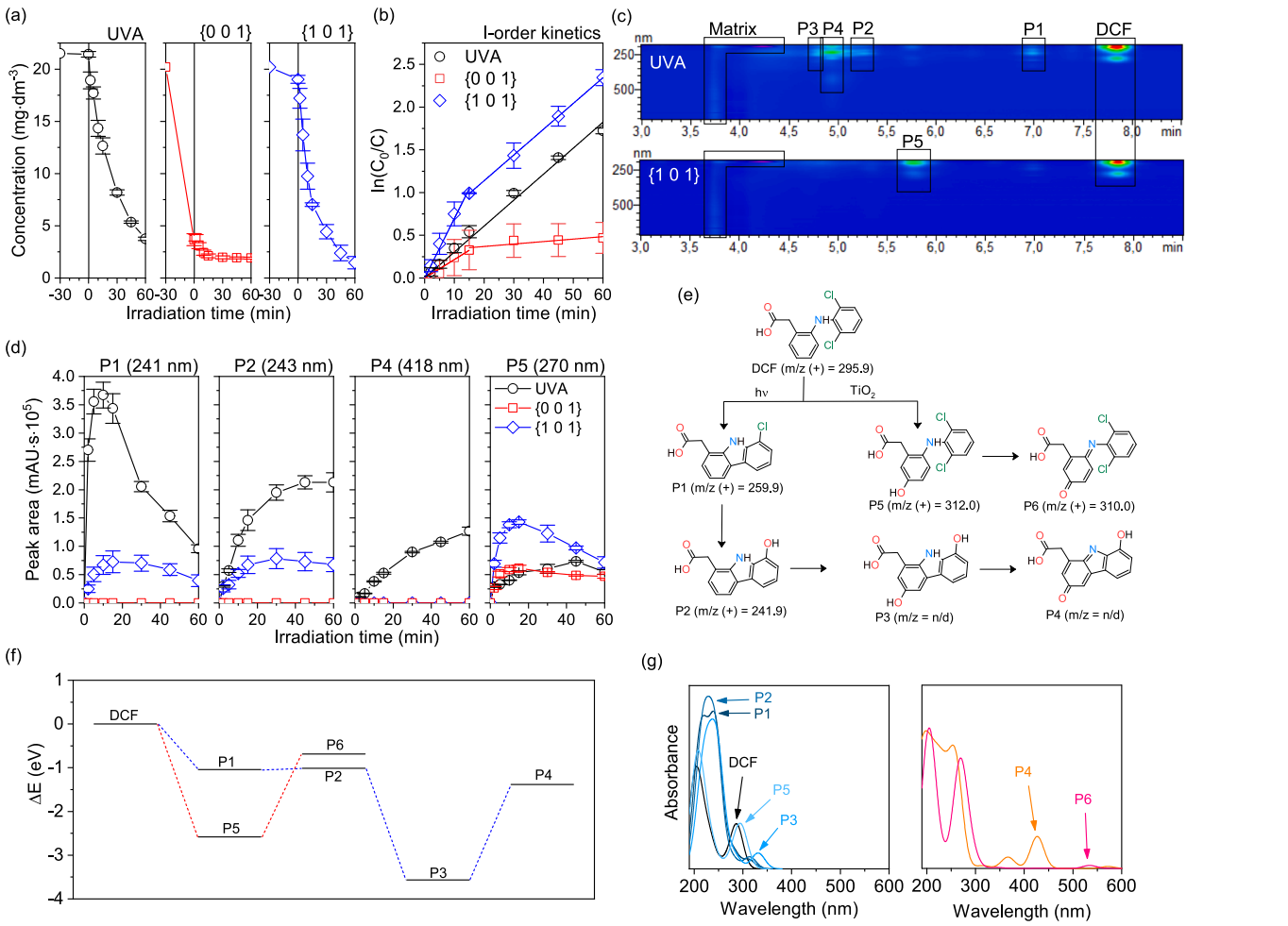

Fig. 4. Observed changes in the diclofenac concentration (a) due to the UVA photolysis and TiO_2-assisted photocatalytic degradation, determined I-order kinetics of the process (b), exemplary DAD chromatograms of the photolysis/photocatalysis process (c), observed accumulation of the selected products over time (d), suggested mechanism of the initial DCF transformation in both processes (e), energy diagram of both initial degradation paths (f) and simulated absorbance spectra of the selected products (g).

analyses due to the acidic separation conditions). Therefore, since almost all DCF became adsorbed before the irradiation, formation of the P1-P4 products became practically eliminated. However, the high adsorption energy might also stabilize the DCF/DCF-OH at the surface, which is not released back to the environment after excitation, leading to the inhibition of the degradation rate for longer irradiation times. On the other hand, the low energy {1 0 1} facets do not show significant in-dark adsorption, leading to the situation where all transformations and adsorption start to occur only after introduction of light. Therefore, mixed photolysis of the free molecules and photocatalytic degradation of photoadsorbed molecules are occurring simultaneously, creating both dehydrohalogenated products P1 and P2, as well as hydroxylated P5.

3.3. *Structure and properties of the Cu modified samples*

Following the above results, clear effects of the TiO_2 presence and its surface structure on the DCF degradation were observed, including the particular role of the in-dark adsorption and UV-induced dehydrohalogenation process. To investigate further possible control over degradation efficiency and its detailed pathway, both TiO_2 materials were surface-modified with Cu clusters/nanoparticles. Copper species are well-known to easily deposit on anatase surfaces under illumination [47], effectively alternating their photocatalytic activity. Due to the low cost of copper, this approach presents a promising and affordable method for TiO_2 modification. However, the detailed effect of the Cu species with respect to the exposed facet has been less investigated compared to isotropic particles, and the impact of the resulting interactions on the degradation process of complex compounds like DCF remains relatively unknown. In this regard, we have studied thoroughly these aspects.

Ultimately, both TiO_2 materials were modified with nominal Cu amounts of 0.5 %, 1 %, 3 % and 5 % (atomic), which were photodeposited under the Xe lamp irradiation from the $CuSO_4$ solution in water/ethanol mixture. In every case, the irradiated solution became pale-purple during the deposition, as presented in Fig. 5a, indicating the formation of the reduced Cu^0 species, with characteristic absorption maximum at approximately 580 nm due to the localized surface plasmon resonance effect (LSPR) [48]. However, after drying, the optical properties of the prepared materials underwent further changes in the span of the next day with a clear shift of the absorption maximum to the higher wavelengths, as presented in Fig. 5b, especially for the lower Cu loadings. Similar maxima were reported previously for the TiO_2/Cu materials and resulted from the oxidation of Cu to the Cu_xO species at the surface [49,50]. Noteworthy, the new maxima at 783 nm and 688 nm are noticeably shifted between both surfaces, indicating the formation of a slightly different band structure in each case, resulting reasonably from the different electronic properties of both surfaces [23,36]. Interestingly, for the Cu loading of 3 % and 5 %, the overall increase of the absorbance in the broad visible light spectrum is clearly observed. This connects with the appearance of metallic copper in the

MOST WIEDZY Downloaded from mostwiedzy.pl

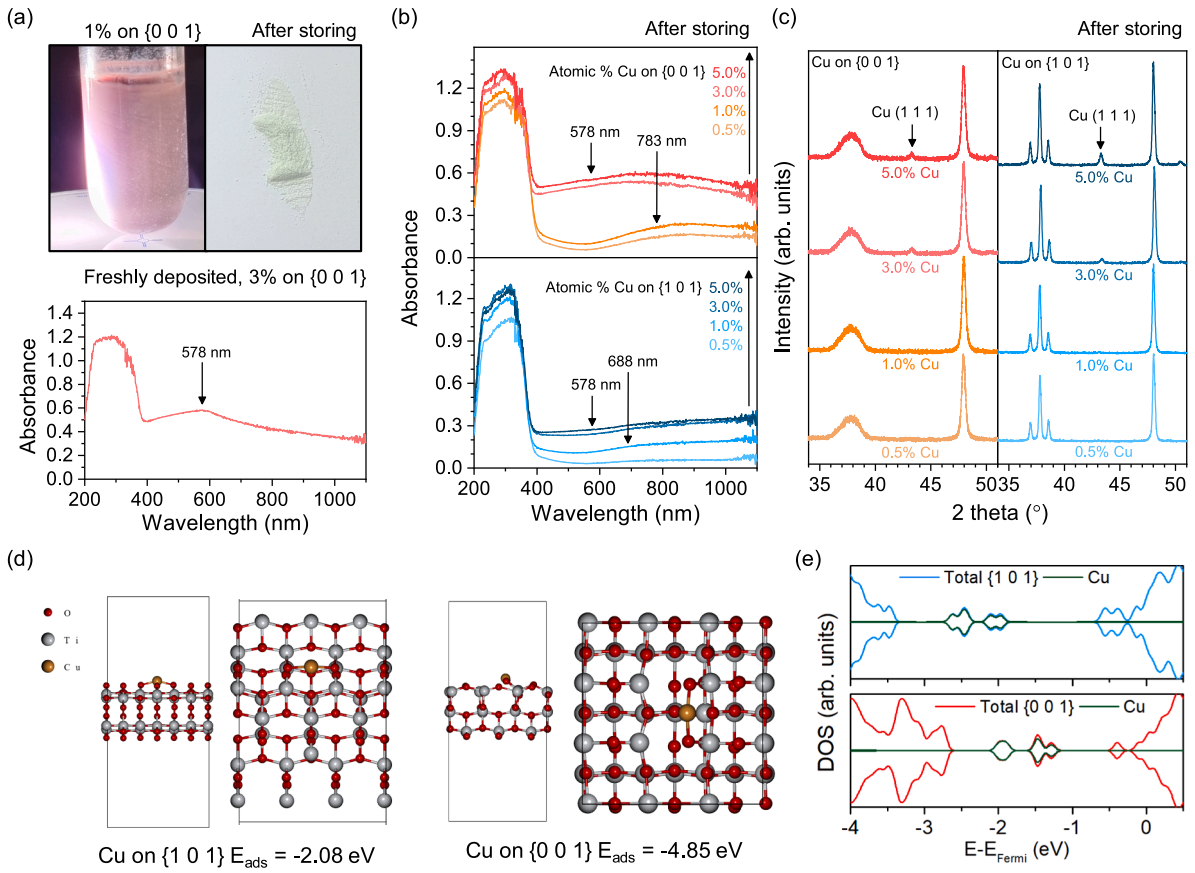

Fig. 5. Exemplary images of the sample color change during the photodeposition and after storing for a few days, with additional absorbance spectrum measured strictly after initial drying of the sample (a); the absorbance spectra of all modified samples after drying and storing (b), corresponding XRD patterns focused on the Cu presence (c), optimized models of the Cu adsorption on both facets with corresponding adsorption energy (d) and calculated DOS distribution for both systems (e).

XRD patterns, as presented in Fig. 5c. The significantly lower signal of the (1 1 1) Cu plane in case of the 5 % modification of the {0 0 1} facets agrees with the high surface development and surface energy of this structure [51], which might improve the dispersion of the Cu species during the deposition. To get better insight into Cu adsorption on both facets, DFT simulations were performed for the periodic slab models of both surfaces with single Cu atom adsorbed. As presented in Fig. 5c, the geometry of Cu adsorption in both cases involve bonding with the 2 of undercoordinated O atoms at the surface. The resulting adsorption energy is exothermic with the high preference of Cu bonding at the {0 0 1} over the {1 0 1} surface (−4.85 eV vs −2.08 eV respectively). Therefore, better dispersion of the Cu species on the {0 0 1} might be expected both due to the high surface area development and high adsorption energy of Cu. Finally, simulated DOS patterns, presented in Fig. 5e, revealed very analogical structure with occupied Cu states adopting energy levels with the bandgap. However, it can be noted that the bandgap of {0 0 1} is visibly reduced, comparing to the {1 0 1}, which is a known to result from the unique electronic structure of the (0 0 1) plane. As the result, Cu states are closer to the CB edge, which might be responsible for the maximum shift observed in the absorbance spectra.

Detailed analysis of the surface presence of Cu and its chemical states were further investigated using XPS spectroscopy. As presented in Fig. 6a, the Cu $2p_{3/2}$ signal can be observed in each case around 932.7 eV, however for the lowest concentrations of 0.5 % at. it is approximately at the detection limit. Further increase of the Cu loading clearly enhances its intensity especially for the {1 0 1} samples, which connects well with the smaller surface area of this material, leading to a visibly higher-than-designed Cu concentrations at the surface (surface Cu/Ti are between 0.9 % and 21 % for this series vs. 0.4 % and 7.5 % for the {0 0 1}). No clear difference in the oxidation state was noticed between the samples, with a single line fitted for the overall signal corresponding to the Cu^0 or Cu^+ oxidation [52].

Outside of the Cu presence, XPS studies have revealed rather similar characteristics between the samples, with detailed results presented in SI (Figs. S4 and S5). However, an increased contribution of the O 1 s signal at ~531.4 eV can be noted for the higher concentrations of Cu (Fig. S5). This signal might origin from the increased presence of oxygen vacancies in the TiO_2 structure, which might affect its photocatalytic activity. In this regard, XPS studies were followed with EPR measurements in order to investigate the formation of possible structural defects. As presented in Fig. 6b, both unmodified materials were found to be relatively defect-free. Specifically, the only signal at g = 2.0034 was noted for the {1 0 1}, which could be ascribed to the hole trapped at the oxygen site [53]. However, concentration of this species is very low, being a few orders of magnitude lower than introduced Cu. Starting from this point, copper introduction results in the appearance of the clear EPR signal around g = 2.1205, which is characteristic for the Cu^{2+} ions [54]. Moreover, in the case of the {0 0 1} with 1 % Cu, the hyperfine structure of the Cu^{2+} was clearly observed with 4 characteristic signals around g = 2.3895 [55,56]. This proves that in this case, Cu exist as the atomically-dispersed species on the surface. For other samples, analogical spectra were not observed and the g = 2.389 signals start to overlap due to the increased dipole–dipole interactions, connected with the reduced distance between neighboring Cu^{2+} centers. In this regard, EPR measurements additionally confirmed better dispersion of the Cu species on the {0 0 1} samples. Interestingly, since only Cu^{2+} can be observed during the EPR measurements, the obtained results stands in some contrast to the XPS, where reduced species were observed. In this regard, we estimated possible concentration of the Cu^{2+} ions from the EPR measurements and compared it to the total amount of introduced

MOST WIEDZY Downloaded from mostwiedzy.pl

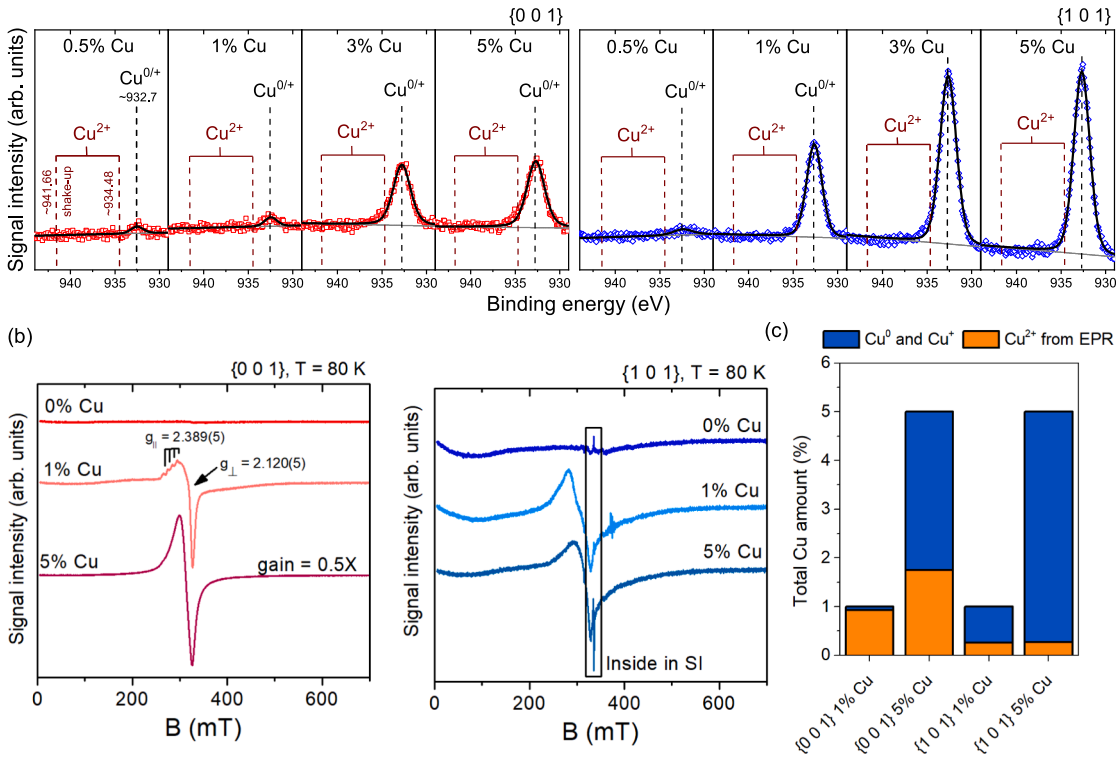

Fig. 6. Deconvolution of the Cu $2p_{3/2}$ XPS signals observed for all modified samples (a), together with the EPR measurements for the bare, 1 % and 5 % modified samples in both series (b) and Cu^{2+} concentration estimated from the EPR measurements, compared to the total amount of introduced Cu (c).

copper. As presented in Fig. 6c, nearly all of the introduced copper might exist as the Cu^{2+} in the case of the {0 0 1} 1 % sample. For other samples however, the amount of Cu^{2+} is not proportional to the overall amount of copper. Based on combined results so far, we conclude that Cu became reduced during the deposition process, and further appearance of the Cu^{2+} resulted from the subsequent oxidation in air. Moreover, in the case of the {0 0 1} facets, high surface area and adsorption energy promote atomic dispersion of the Cu species, which facilities their effective oxidation to Cu^{2+} observed in the EPR spectra. However, both increasing Cu content and changing the material to {1 0 1}, with lower

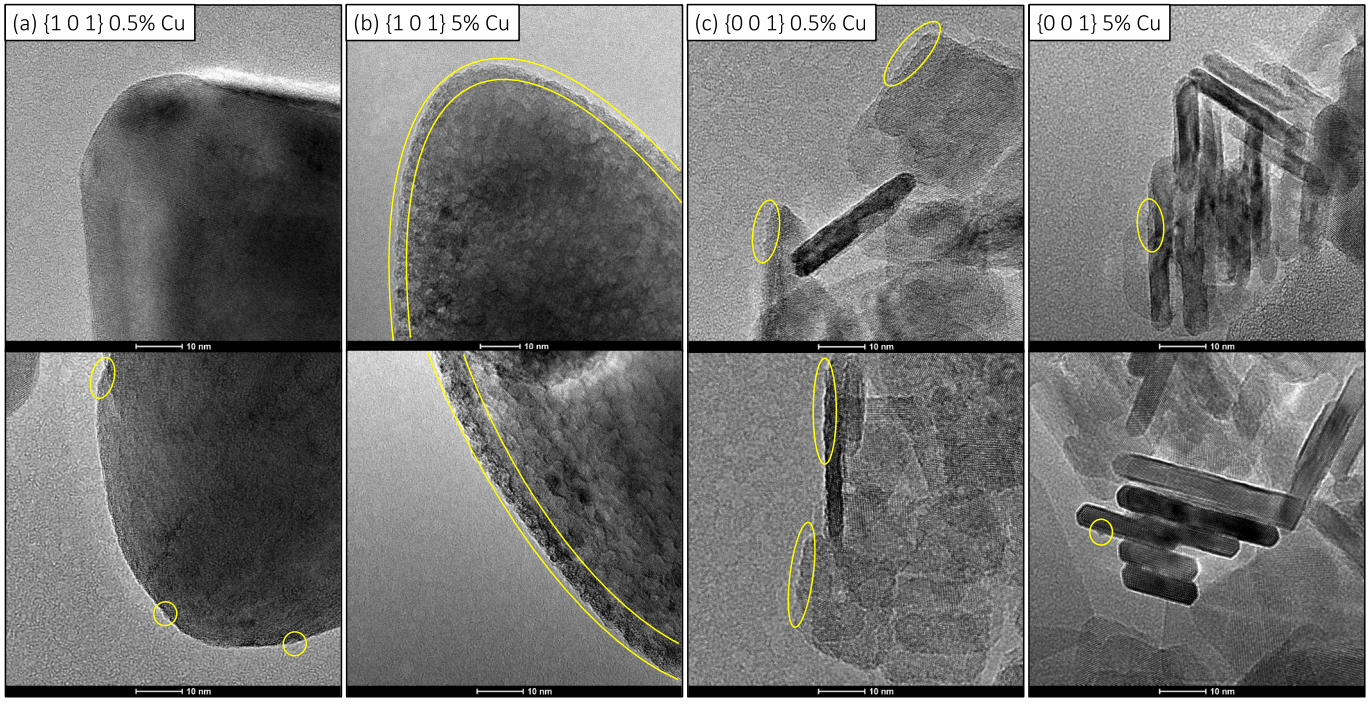

Fig. 7. HR-TEM images of the 0.5 and 5 % Cu-modified samples. Yellow lines highlight exemplary surface irregularities, resulting from the (possible) Cu presence. Scale bars are 10 nm. (For interpretation of the references to color in this figure legend, the reader is referred to the web version of this article.)

MOST WIEDZY Downloaded from mostwiedzy.pl

surface area and weaker interactions with Cu, leads to aggregation of Cu species and stabilize Cu^0/Cu^+ in the final material. Ultimately, we will note that Cu presence has negligible effect on the appearance of other possible EPR signals, although 5 % Cu on {1 0 1} revealed some additional bands for g = 2.0061 and g = 2.0093 (Fig. S7). Therefore, we conclude that ~531.4 eV XPS signal cannot be ascribed in this case to structural defects of TiO_2 and its increase with Cu content results most likely from the post-deposition oxidation of Cu species, leading to different adsorbed O species and mixed oxidation state.

Ultimately, the morphology of the modified materials was investigated in detail for the 0.5 % and 5 % modified samples using TEM observations. As presented in Fig. 7b, in the case of the 5 % modified {1 0 1} particles, the formation of the few-nanometers thick coating of the Cu species is clearly observed, in contrast to the 0.5 % case (Fig. 7a). Noteworthy, no clearly-defined Cu particles were observed in case of other materials, although some surface irregularities, possibly connected with the Cu presence, can be noticed in the range of ≤ 1 nm. Comparing between the {1 0 1} and {0 0 1}, TEM analysis further confirmed better dispersion of the Cu species on the {0 0 1} facets, especially for the higher Cu concentration. For the lower Cu concentrations, no clear formation of any bigger Cu entities was observed, in accordance with the low XPS signals and possible formation of single-atom Cu^{2+} species.

3.4. Degradation of diclofenac over modified samples and •OH generation

Following modification with Cu, obtained materials were tested for diclofenac degradation and compared with the previous observations for unmodified TiO_2. Interestingly, as presented in Fig. 8a, the deposition of Cu had the opposite effect on the activity of both materials, clearly reducing the activity of the {1 0 1} facets and improving it for the {0 0 1}. Furthermore, in the latter case, deposition of the Cu clearly influences the DCF adsorption, as presented in Fig. 8b. This is in accordance with the capping of the adsorption sites with Cu species, which should affect adsorption energy on the (0 0 1) plane. Moreover, as shown in Fig. 8c, modification with Cu also alternated relative concentration of the identified by-products, especially P1 and P5, which were assigned to spontaneous dehydrohalogenation (P1) and hydroxylation due to the reaction with TiO_2 (P5). As observed, especially in the case of {1 0 1} samples, the relative presence of P5 is generally proportional to the degradation rate and also decreases with Cu presence. On the other hand, a slight increase of the P5 formation with Cu is observed for the {0 0 1}, in line with the positive deposition effect on the activity. Focusing on P1, modification with Cu increases its presence for both facets and in the case of the {0 0 1}, its formation is inversely proportional to the observed adsorption. Based on these results, it is concluded that Cu presence decreases activity of the {1 0 1}, which might include a lower ability to generate •OH since reaction with hydroxyl radicals often leads to the formation of hydroxylated products. On the other hand, photocatalytic activity of the {0 0 1} seems to be improved, however high adsorption capacity makes it a bit ambiguous to confirm. In this regard, to better decouple the effect of Cu modification on the adsorption ability and overall photocatalytic activity, additional experiments were performed using coumarin as a probe to detect generated •OH in the system via monitoring of the 7-hydroxycoumarin formation (7–OHC) [57,58]. As presented in Fig. 8d, the observed effect was analogical to the DCF degradation, however the actual maximum of the •OH generation was for the 1 % modified {0 0 1} sample, which was followed by the removal of coumarin itself (Fig. 8e). This suggests that the determined *k* for DCF degradation for this sample was underestimated due to the high adsorption and the optimal Cu loading is somewhere around 1 % Cu/Ti. Interestingly, for the {1 0 1}, the effect of Cu presence is again negative and starting from the concentration of 1 % Cu the formation of

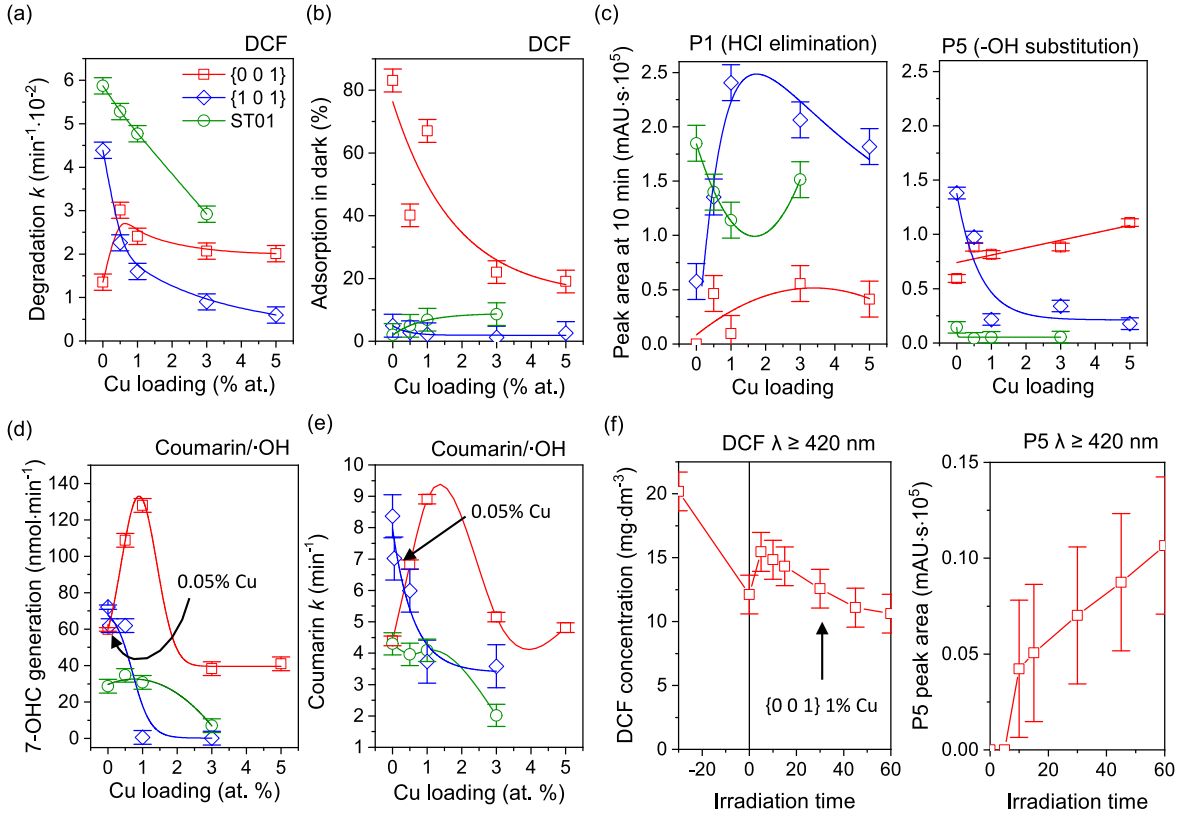

Fig. 8. Effect of Cu loading on the kinetics of diclofenac degradation (a) and in-dark adsorption on the TiO_2 surfaces (b), together with the •OH generation rate (c) determined from the formation of 7-hydroxycoumarin (7–OHC) and corresponding rate of the parent coumarin removal from the solution (d). During the •OH generation, additional {1 0 1} material modified with 0.05% Cu was included to achieve a similar Cu^{2+}/m^2 ratio as for the 0.5% {0 0 1} case.

MOST WIEDZY Downloaded from mostwiedzy.pl

7–hydroxycoumarin was practically stopped, although some removal of the coumarin was still occurring. This results probably from the dense distribution of Cu_XO species on this sample, as clearly evidenced for the 5 % Cu modified sample during TEM observations, which prevents withdrawal of h^+ from the TiO_2 structure. Moreover, since the problem of optimal surface modification connects with the large difference in the determined surface areas between both TiO_2 materials, we have performed additional modification of the {1 0 1} sample with 0.05 % of Cu, in order to achieve a comparable amount of Cu^{2+}/m^2 between {1 0 1} and the 0.5 % modified {0 0 1}. However, as shown in Fig. 8d and 8e, the effect was still negative and overall within the trend. Finally, activity in the visible light ($\lambda \geq 420$ nm) was also tested, focusing on the {0 0 1} with 1 % Cu as the best-performing sample. As shown in Fig. 8f, DCF degradation was initiated under such conditions, which was connected with the appearance of P5 as the only by-product observed in DAD spectra. Furthermore, control experiments confirmed that under these conditions, spontaneous photolysis of DCF is not occurring. However, the observed photocatalytic degradation rate was relatively low, which is a known problem of the TiO_2/Cu_XO systems [59]. Detailed results of the observed kinetics during photocatalytic reactions are presented in Figs. S8 and S9 in SI. Noteworthy, the Cu effect on TOC removal during DCF degradation followed overall trends, achieving the highest removal of 47 % for the 1 % Cu on the {0 0 1}, while for the 1 % Cu on the {1 0 1}, final TOC removal was reduced to 22 % (from 40 %).

Compared to commercial TiO_2, we included analogical modification of anatase ST01 and tested it in both reactions. As presented in Fig. 8, ST01 show high ability to degrade diclofenac, probably connected with its exceptionally high surface development (~300 $m^2 \bullet g^{-1}$). Starting from this point, the introduction of Cu decreases its activity linearly, analogically to the {1 0 1}. Coumarin-based probing of •OH further showed that its generation by ST01 is very low and shows very little change upon Cu modification. This revealed that degradation by ST01 is not dominated by •OH generation and separation of electrons between Cu and ST01 could not increase its activity.

Concerning other studies (Table 1), prepared materials allow to degrade DCF rather effectively, with >90 % of degradation achieved at least within 60 min or faster. For example, the study by Castañeda-Juárez et al. reported only 47 % of degradation over TiO_2-Cu supported on clinoptilolite zeolite after 480 min of irradiation [60]. On the other hand, high degradation rates were reported in systems with high energy radiation, including UVC, as such Hg lamps. Since DCF was found to be prone to UV photolysis, it is likely that this process is also enhanced with high energy radiation included with such light sources.

Concerning stability of the obtained photocatalysts, the best-performing material ({0 0 1} + 1 % Cu) was resynthesized and tested in the 3 consecutive cycles of •OH generation. During these experiments, photocatalyst concentration was increased to 1.5 $g \bullet dm^{-3}$ and the recovered material was washed and dried between each cycle. As presented in Fig. 9a, the material underwent visible activity drop after the first cycle and became stable afterwards. This is further connected with the visible colour change from pale-green to pale-yellow (after the first cycle), with corresponding absorbance spectra shown in Fig. 9b. The new band shows origin approximately at. ~ 2.15 eV, which is a value characteristic of Cu_2O. Transformation of a mixed-valence Cu species deposited on TiO_2 to the Cu_2O after the analogical degradation process was recently reported by Wang et al., who also observed a similar activity decrease after the first reaction [59]. In this regard, it is likely that Cu^{2+} species that are present pre-degradation became reduced to Cu^+ during the reaction. Noteworthy, XPS analysis revealed a slight increase of the reduced copper after the process in accordance with this explanation, as presented in Fig. 9e (please note that due to the separate preparation of {0 0 1} + 1 % Cu for these experiments, detailed Cu dispersion and oxidation state might be slightly different than before, affecting XPS results). No other significant changes were noticed in the XPS spectra. XRD and SEM experiments revealed no visible changes in both materials (Fig. 9c and d).

Following observed activity trends, it is clear that the effect of Cu deposition is strictly opposite for both {0 0 1} and {1 0 1} surfaces, at least when concerning •OH generation and degradation of organic compounds. Interestingly, this was not observed before, despite a rather large interest in the TiO_2/Cu systems. In this regard, a possible explanation is suggested. Recently, reported studies agree that deposition of the Cu_XO species on the TiO_2 forms a Z-scheme junction, which should be especially beneficial for the overall activity under UV excitation [59,70]. In such heterostructure, recombination of charge carriers occurs between the TiO_2 conduction band (e^-) and valence band of Cu_XO (h^+) when irradiated with the UV light. As a result, spatial separation of both carriers is achieved while preserving the high redox ability of the

Table 1
Comparison of the DCF photocatalytic degradation reported in the literature.

Photocatalyst	Photocatalyst concentration	DCF conc.	Irradiation source and intensity	Degradation rate/removal	Ref.
TiO_2-Pd 1 % TiO_2-Ag 1 %	1000 $mg \bullet dm^{-3}$	50 $mg \bullet dm^{-3}$	4x Philips CLEO tubes 15 W, λ_{Max} = 365 nm, 9mW	k = 0.048 min^{-1}, pH = 5 k = 0.040 min^{-1}, pH = 5	[61]
WO_3	250 $mg \bullet dm^{-3}$	0.5 $mg \bullet dm^{-3}$	1500 W Xe lamp, 550 $W \bullet m^{-2}$	100 % after 120 min.	[62]
Supported TiO_2-Cu	10 000 $mg \bullet dm^{-3}$	20 $mg \bullet dm^{-3}$	Solar radiation, UV light = 383.40 ± 0.39 $Wh \bullet m^{-2}$	47 % after 480 min.	[60]
TiO_2	50 $mg \bullet dm^{-3}$	10 $mg \bullet dm^{-3}$	Radium Ralutec, 9 W/78, 350–400 nm 3.37 $\mu einstein \bullet s^{-1}$	85 % after 240 min.	[63]
$SrFeO_3$	300 $mg \bullet dm^{-3}$	50 $mg \bullet dm^{-3}$	Hg vapor lamp 6 W	k = 0.090 min^{-1}	[64]
Graphite/C-doped TiO2	1666 $mg \bullet dm^{-3}$	10 $mg \bullet dm^{-3}$	Short-arc Xe lamp $1.31 \bullet 10^{21}$ photons$\bullet s^{-1}$	k = 0.061 min^{-1}	[65]
ZnO-Ce	1000 $mg \bullet dm^{-3}$	2 $mg \bullet dm^{-3}$	Blacklight Philips TLK 05 40 W λ_{Max} = 360 nm ~30 $W \bullet m^{-2}$	k = 0.110 min^{-1}	[66]
TiO_2	500 $mg \bullet dm^{-3}$	8 $mg \bullet dm^{-3}$	2x Heraeus Hg vapor lamps (low and medium pressure) Flux at 366 nm 2.46 $\mu einstein \bullet s^{-1}$	k = 0.903 min^{-1}	[67]
$ZnO\text{-}WO_3$	800 $mg \bullet dm^{-3}$	20 $mg \bullet dm^{-3}$	Metal halide lamp 400 W	k = 0.013 min^{-1}	[68]
$Sr_{2.7}Nd_{0.3}Fe_{1.4}Co_{0.6}O_{7-\delta}$	100 $mg \bullet dm^{-3}$	20 $mg \bullet dm^{-3}$	Xenon lamp 75 W	100 % after 150 min.	[69]
{1 0 1} TiO_2	500 $mg \bullet dm^{-3}$	20 $mg \bullet dm^{-3}$	Xenon lamp 300 W with IR and 310 nm filter. UVA flux 24 $mW \bullet cm^{-2}$	k = 0.038 min^{-1} 90 % after 60 min	This work
{0 0 1} TiO_2 1 % Cu	400 $mg \bullet dm^{-3}$			k = 0.024 min^{-1} 90 % after 30 min	
ST01 TiO_2				k = 0.059 min^{-1} 100 % after 45 min	

MOST WIEDZY Downloaded from mostwiedzy.pl

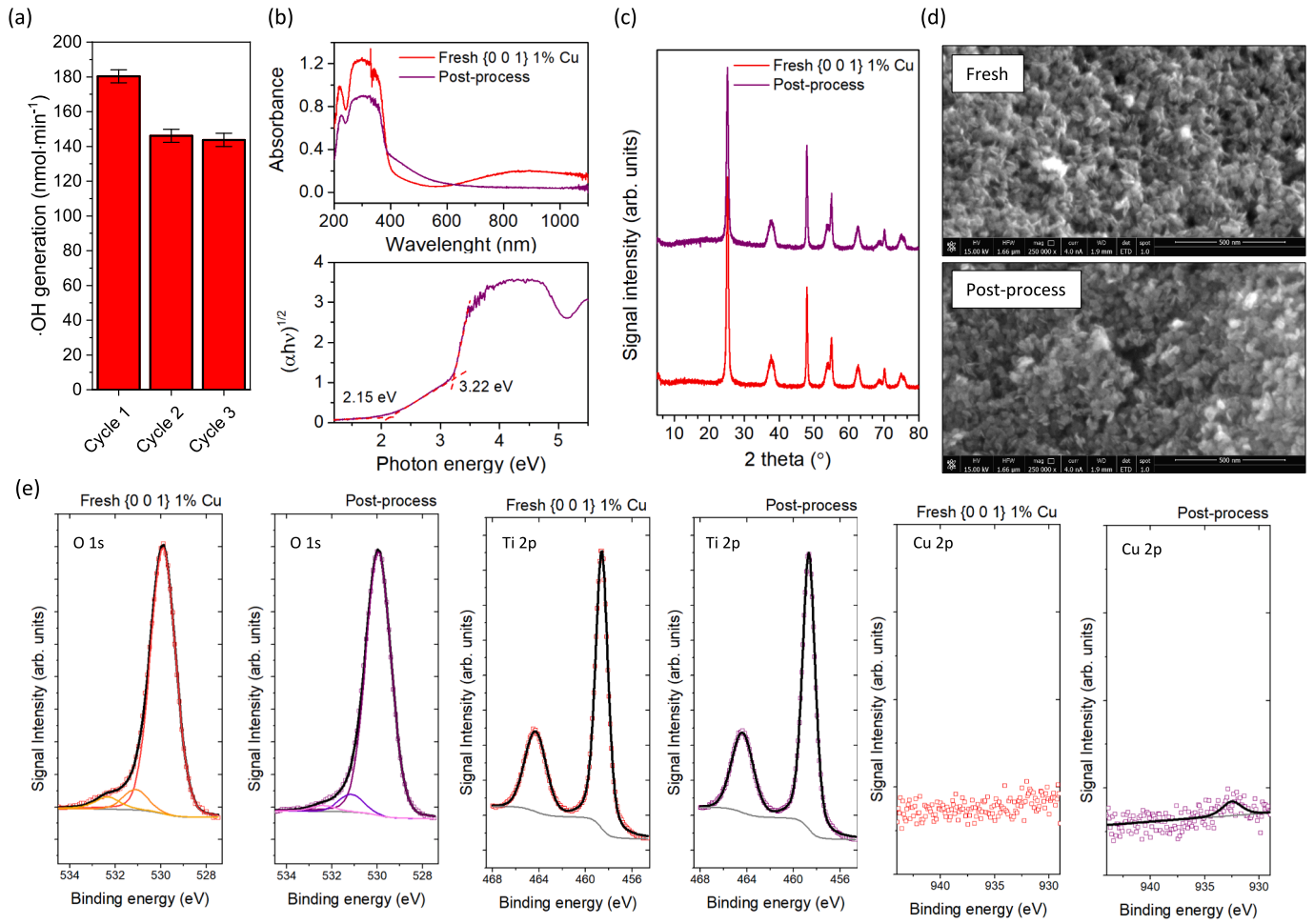

Fig. 9. Stability tests of the {0 0 1} + 1 % Cu sample during •OH generation (a) with corresponding characteristics before and after the process: absorbance (b), XRD (c), SEM (d) and XPS (e). Please note that new sample was prepared for these experiments and some differences from previous results might be present.

Cu_XO electrons and TiO_2 holes. Outside of the clear reduction of copper observed in the XPS spectra, we have additionally confirmed this separation with the photoluminescence spectra measurements, confirming that increased Cu loading reduces emission around ~450 nm, which should occur due to the electron-hole recombination within the TiO_2 structure. As shown in Fig. 10a, the effect is the same for both TiO_2 facets. In this regard, effective charge separation is occurring in both systems. In the case of {0 0 1} facets, this straightforwardly increases photocatalytic activity, including •OH generation, which should mostly result from the h^+ induced oxidation of water/hydroxyl groups present on the TiO_2 surface (please note that valence band potentials of Cu oxides are too low to effectively generate •OH from H_2O or –OH [71–77]). Noteworthy, due to the high surface energy, it is known that H_2O can spontaneously dissociate on the {0 0 1} surface, forming multiple –OH, which are particularly good substrates for h^+ oxidation due to the higher electron density [78]. On the contrary, the reduction ability of the {0 0 1} is generally worse than other TiO_2 surfaces, due to its unfavored electronic structure compared to the bulk [9,23]. In this regard, "shifting" the reduction reaction to Cu_XO might be additionally beneficial for the overall activity. On the other hand, the reduction process is important for the {1 0 1} facets, which preferentially trap electrons on the surface sites [79]. Particularly, this connects with the increased hydroxylation of this surface due to the electron-induced water dissociation [80], which otherwise is partially limited. As a consequence, oxygen reduction contribute also to the •OH generation [81], and some excess electrons are important for the surface hydroxylation and h^+ trapping [82]. In this regard, the Z-scheme recombination of the TiO_2 electrons reasonably reduces the overall activity of the {1 0 1} facets, since oxygen reduction must be hindered at this surface. The scheme of these processes (charge separation and ROS generation in water/air) is presented in Fig. 10c, based on the known information about band position of TiO_2 and Cu_2O [83–87]. Interestingly, we have also tested obtained materials in the reaction of 4-nitrophenol reduction to 4-aminophenol in methanol, to verify if the Cu effect on other reduction process would be analogical. However, as presented in Fig. 10b, the effect was negative in both cases and Cu clearly reduced amount of 4-aminophenol evolved. This show that deposited Cu_XO species cannot be seen as universal reduction co-catalyst and they are especially beneficial for the degradation process when combined with the {0 0 1} facets. Ultimately, these results suggest that the same Z–scheme junction might have different effect on the photocatalytic activity, depending on the electronic structure and reactions details occurring on the TiO_2 surface, which was clearly presented for the first time.

4. Conclusions

In the present work, detailed insight into the complex effects of Cu_XO loading at the {0 0 1} and {1 0 1} crystal facets of TiO_2 and how it affects photodegradation of diclofenac (DCF), generation of •OH and 4-nitrophenol reduction were investigated. Overall results have presented the existence of two independent degradation pathways, either dehydrohalogenation or hydroxylation, both of them sensitive to different factors. Specifically, dehydrohalogenation occurs spontaneously in the solution under irradiation with suitable light (UVA range), leading to the

MOST WIEDZY Downloaded from mostwiedzy.pl

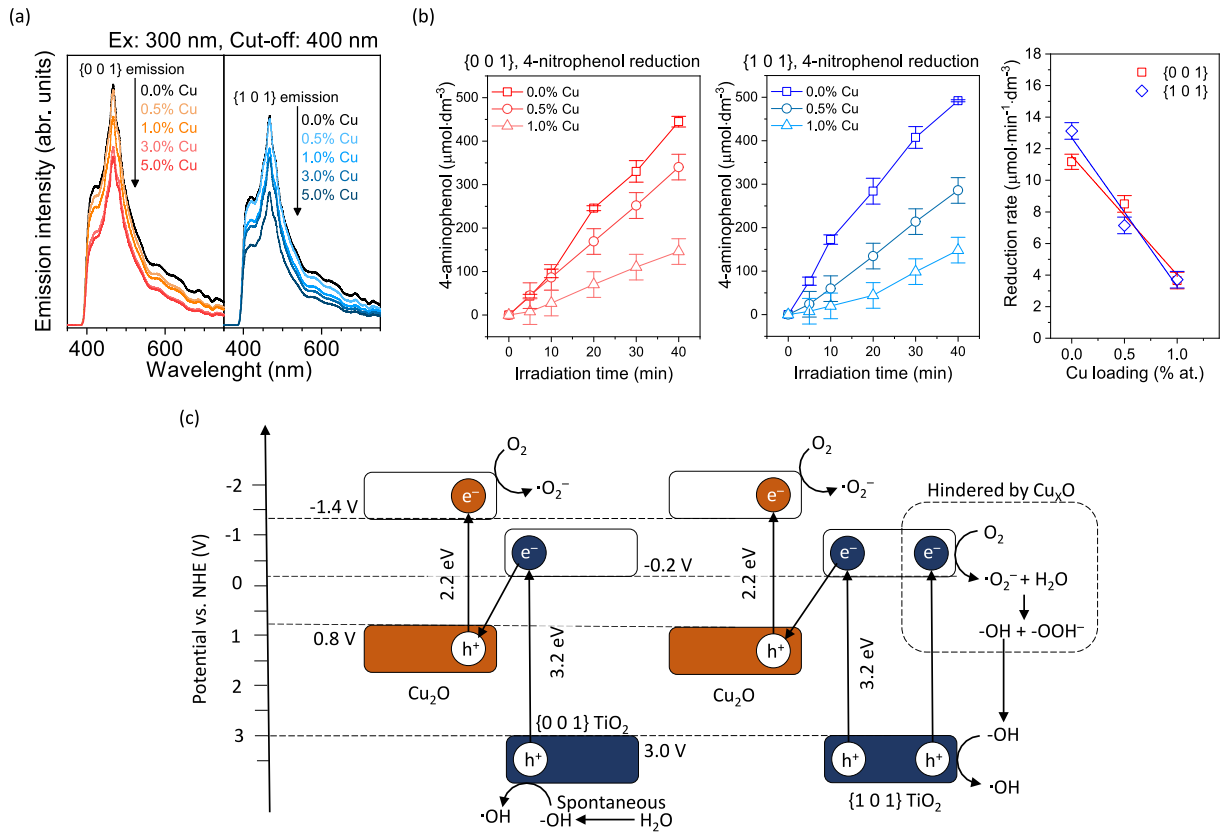

Fig. 10. Recorded photoluminescence spectra of the bare and Cu-modified materials after excitation with UV light (a), results of the 4-nitrphenol reduction (b) and proposed scheme of the possible reactions and charge separation during the diclofenac photooxidation in water (c). In case of the {1 0 1} facets, the scheme in (c) include dissociation of water due to the oxygen reduction on the unmodified surface, which was recently recognized as important for the {1 0 1} activity.

formation of carbazole derivatives. On the other hand, in the presence of TiO_2 photocatalyst, DCF hydroxylation is preferentially occurring. Selectivity of both these processes depends strongly on light energy, as well as on the DCF adsorption on TiO_2 surface. Noteworthy, high DCF adsorption was observed for the {0 0 1} facets, which led to almost selective formation of hydroxylated product. Following this, a very strong effect of Cu_XO in all systems were observed with quantitively different effects in the case of •OH generation and DCF degradation. From overall results, the synergy of Cu_XO cooperation with {0 0 1} facets in both these reactions was clearly observed, e.g. boosting their ability to generate •OH over 2-times. Combination of EPR, XRD and XPS studies revealed that depending on the Cu concentration and type of the surface, different amounts of $Cu^{2+}/Cu^{+}/Cu^{0}$ can be observed in the system. For the most active material ({0 0 1} with 1 % Cu), copper exists mostly as the atomically-scattered Cu^{2+} species, which are later transferred to the Cu_2O during the degradation. Such atomic dispersion is a combined effect of high Cu adsorption energy and high surface development of the {0 0 1} exposing materials. Interestingly, we were not able to recreate analogical effect on the activity of the {1 0 1}, despite testing Cu concentration over 3 orders of magnitude (from 0.05 % to 5 %). Therefore, despite forming the same Z-scheme junction in both cases, the qualitative effect of Cu_XO deposition was found to be different for both facets in these reactions. This is explained to result from the different roles of both e^- and h^+ on the generation of reactive species on both {0 0 1} and {1 0 1}, where electrons are especially needed to stimulate the activity of the {1 0 1}, including generation of •OH. Concerning 4-nitrophenol reduction, Cu_XO presence decreased its efficiency for both systems, proving that synergy between copper and {0 0 1} facets are unique for the ROS generation.

CRediT authorship contribution statement

Szymon Dudziak: Writing – review & editing, Writing – original draft, Methodology, Investigation, Formal analysis, Conceptualization. **Jakub Smoliński:** Writing – original draft, Investigation, Formal analysis. **Adam Ostrowski:** Writing – original draft, Methodology, Investigation, Formal analysis. **Aleksandra Szkudlarek:** Writing – review & editing, Methodology, Investigation, Formal analysis. **Mateusz Marzec:** Writing – review & editing, Methodology, Investigation, Formal analysis. **Krystian Sokołowski:** Writing – review & editing, Methodology, Investigation, Formal analysis. **Karol Sikora:** Methodology, Investigation, Formal analysis. **Anna Zielińska-Jurek:** Supervision, Resources, Project administration, Methodology, Funding acquisition, Conceptualization.

Declaration of competing interest

The authors declare the following financial interests/personal relationships which may be considered as potential competing interests: Anna Zielinska-Jurek reports financial support was provided by National Science Centre Poland. Szymon Dudziak reports financial support was provided by Foundation for Polish Science. If there are other authors, they declare that they have no known competing financial interests or personal relationships that could have appeared to influence the work reported in this paper.

Acknowledgements

This work was financially supported by the Polish National Science Centre, with grant no. NCN 2021/43/B/ST5/02983 and by the Gdańsk University of Technology within the RADIUM program (DEC 15/

MOST WIEDZY Downloaded from mostwiedzy.pl

RADIUM/2022). SD acknowledges financial support from the Foundation for Polish Science (FNP) with the START program.

Appendix A. Supplementary data

Supplementary data to this article can be found online at https://doi.org/10.1016/j.cej.2024.159146.

Data availability

Data will be made available on request.

References

[1] C.Y. Chang, A. Yamakata, W.J. Tseng, Effect of surface plasmon resonance and the heterojunction on photoelectrochemical activity of metal-loaded TiO_2 electrodes under visible light irradiation, J. Phys. Chem. C 126 (30) (2022) 12450–12459, https://doi.org/10.1021/acs.jpcc.2c02649.

[2] J. Guo, L. Song, M. Chen, F. Mo, W. Yu, Y. Fu, Schottky-functionalized Z-scheme heterojunction: improved photoelectric conversion efficiency and immunosensing, Biosens. Bioelectron. 222 (115000) (2023) 0956–5663, https://doi.org/10.1016/j.bios.2022.115000.

[3] M. Humayun, F. Raziq, A. Khan, W. Luo, Modification strategies of TiO_2 for potential applications in photocatalysis: a critical review, Green Chem. Lett. Rev. 11 (2) (2018) 86–102, https://doi.org/10.1080/17518253.2018.1440324.

[4] H.W.P. Carvalho, A.P.L. Batista, P. Hammer, T.C. Ramalho, Photocatalytic degradation of methylene blue by TiO_2–Cu thin films: theoretical and experimental study, J. Hazard. Mater. 184 (1–3) (2010) 273–280, https://doi.org/10.1016/j.jhazmat.2010.08.033.

[5] C. Günnemann, C. Haisch, M. Fleisch, J. Schneider, A.V. Emeline, D. W. Bahnemann, Insights into different photocatalytic oxidation activities of anatase, brookite, and rutile single-crystal facets, ACS Catal. 9 (2019) 1001–1012, https://doi.org/10.1021/acscatal.8b04115.

[6] M.P. Jiang, K.K. Huang, J.H. Liu, D. Wang, Y. Wang, X. Wang, Z.D. Li, X.Y. Wang, Z.B. Geng, X.Y. Hou, S.H. Feng, Magnetic-field-regulated TiO_2 100 facets: a strategy for C-C coupling in CO_2 photocatalytic conversion, Chem 6 (2020) 2335–2346, https://doi.org/10.1016/j.chempr.2020.06.033.

[7] R. Katal, S. Masudy-Panah, M. Tanhaei, M.H.D.A. Farahani, H. Jiangyong, A review on the synthesis of the various types of anatase TiO_2 facets and their applications for photocatalysis, Chem. Eng. J. 384 (2020) 123384, https://doi.org/10.1016/j.cej.2019.123384.

[8] S. Dudziak, E. Kowalska, K. Wang, J. Karczewski, M. Sawczak, B. Ohtani, A. Zielińska-Jurek, The interplay between dopant and a surface structure of the photocatalyst – The case study of Nb-doped faceted TiO_2, Appl. Catal. B Environ. 328 (2023), https://doi.org/10.1016/j.apcatb.2023.122448.

[9] S. Selcuk, A. Selloni, Facet-dependent trapping and dynamics of excess electrons at anatase TiO_2 surfaces and aqueous interfaces, Nat. Mater. 15 (2016) 1107–1112, https://doi.org/10.1038/nmat4672.

[10] H. Chen, J.A. Dawson, N. Umezawa, Anisotropic nature of anatase TiO_2 and its intrinsic (001) surface electronic states, PhysRevAppli 4 (2015) 014007, https://doi.org/10.1103/PhysRevApplied.4.014007.

[11] D. Wang, X.Q. Gong, Function-oriented design of robust metal cocatalyst for photocatalytic hydrogen evolution on metal/titania composites, Nat. Commun. 12 (2021) 1–6, https://doi.org/10.1038/s41467-020-20464-x.

[12] F. Yu, X. Wang, H. Lu, G. Li, B. Liao, H. Wang, C. Duan, Y. Mao, L. Chen, Surface engineering of TiO_2 nanosheets to boost photocatalytic methanol dehydrogenation for hydrogen evolution, Inorg. Chem. 62 (2023) 5700–5706, https://doi.org/10.1021/acs.inorgchem.3c00250.

[13] X. Hu, J. Song, J. Luo, H. Zhang, Z. Sun, C. Li, S. Zheng, Q. Liu, Single-atomic Pt sites anchored on defective TiO_2 nanosheets as a superior photocatalyst for hydrogen evolution, J. Energy Chem. 62 (2021) 1–10, https://doi.org/10.1016/j.jechem.2021.03.003.

[14] J. Yu, L. Qi, M. Jaroniec, Hydrogen production by photocatalytic water splitting over Pt/TiO_2 nanosheets with exposed (001) facets, J. Phys. Chem. C 114 (2010) 13118–13125, https://doi.org/10.1021/jp104488b.

[15] Z. Wei, M. Janczarek, M. Endo, K. Wang, A. Balčytis, A. Nitta, M.G. Méndez-Medrano, C. Colbeau-Justin, S. Juodkazis, B. Ohtani, E. Kowalska, Noble metal-modified faceted anatase titania photocatalysts: octahedron versus decahedron, Appl. Catal. B Environ. 237 (2018) 574–587, https://doi.org/10.1016/j.apcatb.2018.06.027.

[16] L. Lonappan, S.K. Brar, R.K. Das, M. Verma, R.Y. Surampalli, Diclofenac and its transformation products: environmental occurrence and toxicity - A review, Environ. Int. 96 (2016) 127–138, https://doi.org/10.1016/j.envint.2016.09.014.

[17] P. McGettigan, D. Henry, Use of non-steroidal anti-inflammatory drugs that elevate cardiovascular risk: an examination of sales and essential medicines lists in low-, middle-, and high-income countries, PLoS Med. 10 (2) (2013) e1001388, https://doi.org/10.1371/journal.pmed.1001388.

[18] B. Bonnefille, E. Gomez, F. Courant, A. Escande, H. Fenet, Diclofenac in the marine environment: a review of its occurrence and effects, Mar. Pollut. Bull. 131 (2018) 496–506, https://doi.org/10.1016/j.marpolbul.2018.04.053.

[19] W. Schmidt, K. O'Rourke, R. Hernan, B. Quinn, Effects of the pharmaceuticals gemfibrozil and diclofenac on the marine mussel (Mytilus spp.) and their comparison with standardized toxicity tests, Mar. Pollut. Bull. 62 (7) (2011) 1389–1395, https://doi.org/10.1016/j.marpolbul.2011.04.043.

[20] W. Schmidt, L.C. Rainville, G. McEneff, D. Sheehan, B. Quinn, A proteomic evaluation of the effects of the pharmaceuticals diclofenac and gemfibrozil on marine mussels (Mytilus spp.): evidence for chronic sublethal effects on stress-response proteins, Drug Test Analysis 6 (2014) 210–219, https://doi.org/10.1002/dta.1463.

[21] C. Ribalta, M. Solé, In vitro interaction of emerging contaminants with the cytochrome P450 system of mediterranean deep-sea fish, Environ. Sci. Tech. 48 (20) (2014) 12327–12335, https://doi.org/10.1021/es5029603.

[22] N.B.M. Zanuri, M.G. Bentley, G.S. Caldwell, Assessing the impact of diclofenac, ibuprofen and sildenafil citrate (Viagra®) on the fertilisation biology of broadcast spawning marine invertebrates, Mar. Environ. Res. 127 (126–136) (2017) 0141–1136, https://doi.org/10.1016/j.marenvres.2017.04.005.

[23] F. Cuklev, E. Kristiansson, J. Fick, N. Asker, L. Förlin, D.G.J. Larsson, Diclofenac in fish: blood plasma levels similar to human therapeutic levels affect global hepatic gene expression, Environ. Toxicol. Chem. 30 (9) (2011) 2126–2134, https://doi.org/10.1002/etc.599.

[24] F. Amano, T. Yasumoto, O.O. Prieto-Mahaney, S. Uchida, T. Shibayama, B. Ohtani, Photocatalytic activity of octahedral single-crystalline mesoparticles of anatase titanium(IV) oxide, Chem. Commun. (2009) 2311–2313, https://doi.org/10.1039/b822634b.

[25] S. Dudziak, M. Kowalkińska, J. Karczewski, M. Pisarek, K. Siuzdak, A. Kubiak, K. Siwińska-Ciesielczyk, A. Zielińska-Jurek, Solvothermal growth of 0 0 1 exposed anatase nanosheets and their ability to mineralize organic pollutants. The effect of alcohol type and content on the nucleation and growth of TiO_2 nanostructures, Appl. Surf. Sci. 563 (2021) 150360, https://doi.org/10.1016/j.apsusc.2021.150360.

[26] J. Li, D. Xu, Tetragonal faceted-nanorods of anatase TiO_2 single crystals with a large percentage of active 100 facets, Chem. Commun. 46 (2010) 2301–2303, https://doi.org/10.1039/b923755k.

[27] A. Brucato, A.E. Cassano, F. Grisafi, G. Montante, L. Rizzuti, G. Vella, Estimating radiant fields in flat heterogeneous photoreactors by the six-flux model, AIChE J. 52 (2006) 3882–3890, https://doi.org/10.1002/aic.10984.

[28] I. Grčić, G. Li Puma, Photocatalytic degradation of water contaminants in multiple photoreactors and evaluation of reaction kinetic constants independent of photon absorption, irradiance, reactor geometry, and hydrodynamics, Environ. Sci. Technol. 47 (2013) 13702–13711, https://doi.org/10.1021/es403472e.

[29] R. Acosta-Herazo, J. Monterroza-Romero, M.Á. Mueses, F. Machuca-Martínez, G. Li Puma, Coupling the six flux absorption-scattering model to the henyey-greenstein scattering phase function: evaluation and optimization of radiation absorption in solar heterogeneous photoreactors, Chem. Eng. J. 302 (2016) 86–96, https://doi.org/10.1016/j.cej.2016.04.127.

[30] F. Neese, Software update: the ORCA program system—Version 5.0, Wiley Interdiscip. Rev. Comput. Mol. Sci. (2022) 1–15, https://doi.org/10.1002/wcms.1606.

[31] P. Giannozzi, O. Andreussi, T. Brumme, O. Bunau, M. Buongiorno Nardelli, M. Calandra, R. Car, C. Cavazzoni, D. Ceresoli, M. Cococcioni, N. Colonna, I. Carnimeo, A. Dal Corso, S. De Gironcoli, P. Delugas, R.A. DiStasio Jr, A. Ferretii, A. Floris, G. Fratesi, G. Fugallo, R. Gebauer, U. Gerstmann, F. Giustino, T. Gorni, J. Jia, M. Kawamura, H.-Y. Ko, A. Kokalj, E. Küçükbenli, M. Lazzeri, M. Marsili, N. Marzani, F. Mauri, N.L. Nguyen, H.-V. Nguyen, A. Otero-de-la-Roza, L. Paulatto, S. Poncé, D. Rocca, R. Sabatini, B. Santra, M. Schlipf, A.P. Seitsonen, A. Smogunov, I. Timrov, T. Thonhauser, P. Umari, N. Vast, X. Wu, S. Baroni, Advanced capabilities for materials modelling with Quantum Espresso, J. Phys. Condens. Matter 29 (2017) 465901.

[32] S.A. Hassanzadeh-Tabrizi, Precise calculation of crystallite size of nanomaterials: a review, J. Alloys Compd. 968 (2023) 171914, https://doi.org/10.1016/j.jallcom.2023.171914.

[33] C. Xia, W. Wu, T. Yu, X. Xie, C. Van Oversteeg, H.C. Gerritsen, C. De Mello Donega, Size-dependent band-gap and molar absorption coefficients of colloidal CuInS2 quantum dots, ACS Nano 12 (2018) 8350–8361, https://doi.org/10.1021/acsnano.8b03641.

[34] M. Singh, M. Goyal, K. Devlal, Size and shape effects on the band gap of semiconductor compound nanomaterials, J. Taibah Univ. Sci. 12 (2018) 470–475, https://doi.org/10.1080/16583655.2018.1473946.

[35] S. Monticone, R. Tufeu, A.V. Kanaev, E. Scolan, C. Sanchez, F.F. Francé, Quantum size effect in TiO nanoparticles: does it exist?, n.d. www.elsevier.nlrlocaterapsusc.

[36] Z. Zhao, Z. Li, Z. Zou, Surface properties and electronic structure of low-index stoichiometric anatase TiO_2 surfaces, J. Phys. Condens. Matter 22 (2010) 175008, https://doi.org/10.1088/0953-8984/22/17/175008.

[37] H. Ariga, T. Taniike, H. Morikawa, M. Tada, K.M. Byoung, K. Watanabe, Y. Matsumoto, S. Ikeda, K. Saiki, Y. Iwasawa, Surface-mediated visible-light photo-oxidation on pure TiO_2 (001), J. Am. Chem. Soc. 131 (2009) 14670–14672, https://doi.org/10.1021/ja9066805.

[38] T.R. Gordon, M. Cargnello, T. Paik, F. Mangolini, R.T. Weber, P. Fornasiero, C. B. Murray, Nonaqueous synthesis of TiO_2 nanocrystals using TiF_4 to engineer morphology, oxygen vacancy concentration, and photocatalytic activity, J. Am. Chem. Soc. 134 (2012) 6751–6761, https://doi.org/10.1021/ja300823a.

[39] M. Kowalkińska, K. Sikora, M. Łapiński, J. Karczewski, A. Zielińska-Jurek, Non-toxic fluorine-doped TiO_2 nanocrystals from $TiOF_2$ for facet-dependent naproxen degradation, Catal. Today 413–415 (2022) 113959, https://doi.org/10.1016/j.cattod.2022.11.020.

[40] Q. Xiang, K. Lv, J. Yu, Pivotal role of fluorine in enhanced photocatalytic activity of anatase TiO_2 nanosheets with dominant (0 0 1) facets for the photocatalytic

MOST WIEDZY Downloaded from mostwiedzy.pl

degradation of acetone in air, Appl. Catal. B Environ. 96 (2010) 557–564, https://doi.org/10.1016/j.apcatb.2010.03.020.
[41] A.V. Romanov, M.A. Yurkin, Single-particle characterization by elastic light scattering, Laser Photonics Rev. 15 (2021), https://doi.org/10.1002/lpor.202000368.
[42] E. Mrotek, S. Dudziak, I. Malinowska, D. Pelczarski, Z. Ryżyńska, A. Zielińska-Jurek, Improved degradation of etodolac in the presence of core-shell $ZnFe_2O_4$/SiO_2/TiO_2 magnetic photocatalyst, Sci. Total Environ. 724 (2020) 1–12, https://doi.org/10.1016/j.scitotenv.2020.138167.
[43] H.G. Yang, C.H. Sun, S.Z. Qiao, J. Zou, G. Liu, S.C. Smith, H.M. Cheng, G.Q. Lu, Anatase TiO_2 single crystals with a large percentage of reactive facets, Nature 453 (2008) 638–641, https://doi.org/10.1038/nature06964.
[44] W.J.I. DeBenedetti, E.S. Skibinski, D. Jing, A. Song, M.A. Hines, Atomic-scale understanding of catalyst activation: carboxylic acid solutions, but not the acid itself, increase the reactivity of anatase (001) faceted nanocatalysts, J. Phys. Chem. C 122 (2018) 4307–4314, https://doi.org/10.1021/acs.jpcc.7b11054.
[45] G. Zeng, B. Wen, A. Selloni, Structure and stability of pristine and carboxylate-covered anatase TiO_2(001) in aqueous environment, J. Phys. Chem. C 125 (2021) 15910–15917, https://doi.org/10.1021/acs.jpcc.1c03623.
[46] F. Roncaroli, M.A. Blesa, Kinetics of adsorption of carboxylic acids onto titanium dioxide, Phys. Chem. Chem. Phys. 12 (2010) 9938–9944, https://doi.org/10.1039/c003086d.
[47] Z. Bielan, E. Kowalska, S. Dudziak, K. Wang, B. Ohtani, A. Zielińska-Jurek, Mono- and bimetallic (Pt/Cu) titanium(IV) oxide core–shell photocatalysts with UV/Vis light activity and magnetic separability, Catal. Today 361 (2021) 198–209, https://doi.org/10.1016/j.cattod.2020.05.034.
[48] G.-Y. Yao, Z.-Y. Zhao, Q.-L. Liu, X.-D. Dong, Q.-M. Zhao, Theoretical calculations for localized surface plasmon resonance effects of Cu/TiO_2 nanosphere: generation, modulation, and application in photocatalysis, Sol. Energy Mater. Sol. Cells 208 (2020) 110385, https://doi.org/10.1016/j.solmat.2019.110385.
[49] K. Ćwieka, Z. Bojarska, K. Czelej, D. Łomot, P. Dziegielewski, A. Maximenko, K. Nikiforow, L. Gradoń, M.Y. Qi, Y.J. Xu, J.C. Colmenares, Zero carbon footprint hydrogen generation by photoreforming of methanol over Cu/TiO_2 nanocatalyst, Chem. Eng. J. 474 (2023), https://doi.org/10.1016/j.cej.2023.145687.
[50] V. Polliotto, S. Livraghi, A. Krukowska, M.V. Dozzi, A. Zaleska-Medynska, E. Selli, E. Giamello, Copper-modified TiO_2 and $ZrTiO_4$: Cu oxidation state evolution during photocatalytic hydrogen production, ACS Appl. Mater. Interfaces 10 (2018) 27745–27756, https://doi.org/10.1021/acsami.8b05528.
[51] M. Lazzeri, A. Vittadini, A. Selloni, Structure and energetics of stoichiometric TiO_2 anatase surfaces, Phys. Rev. B - Condens. Matter Mater. Phys. 63 (2001) 1554091–1554099, https://doi.org/10.1103/PhysRevB.63.155409.
[52] M.C. Biesinger, L.W.M. Lau, A.R. Gerson, R.St.C. Smart, Resolving surface chemical states in XPS analysis of first row transition metals, oxides and hydroxides: Sc, Ti, V, Cu and Zn, Appl. Surf. Sci. 257 (2010) 887–898, https://doi.org/10.1016/j.apsusc.2010.07.086.
[53] O. Al-Madanat, Y. AlSalka, R. Dillert, D.W. Bahnemann, Photocatalytic H_2 production from naphthalene by various TiO_2 photocatalysts: impact of Pt loading and formation of intermediates, Catalysts 11 (2021) 107, https://doi.org/10.3390/catal11010107.
[54] A. Zollo, V. Polliotto, S. Livraghi, E. Giamello, Self-organisation of copper species at the surface of Cu–TiO_2 systems during H_2 evolution reaction: a combined investigation by EPR and optical spectroscopy, Appl. Magn. Reson. 51 (2020) 1497–1513, https://doi.org/10.1007/s00723-020-01226-w.
[55] T. Wang, F. Sun, S. Liu, G. Zhuang, B. Li, Dioxygen-enhanced CO_2 photoreduction on TiO_2 supported Cu single-atom sites, Appl. Catal. B Environ. 325 (2023) 122339, https://doi.org/10.1016/j.apcatb.2022.122339.
[56] K. Kruczała, S. Neubert, K. Dhaka, D. Mitoraj, P. Jánošíková, C. Adler, I. Krivtsov, J. Patzsch, J. Bloh, J. Biskupek, U. Kaiser, R.K. Hocking, M. Caspary Toroker, R. Beranek, Enhancing photocatalysis: understanding the mechanistic diversity in photocatalysts modified with single-atom catalytic sites, Adv. Sci. 10 (2023) 2303571, https://doi.org/10.1002/advs.202303571.
[57] J. Zhang, Y. Nosaka, Photocatalytic oxidation mechanism of methanol and the other reactants in irradiated TiO_2 aqueous suspension investigated by OH radical detection, Appl. Catal. B Environ. 166–167 (2015) 32–36, https://doi.org/10.1016/j.apcatb.2014.11.006.
[58] A. Wafi, E. Szabó-Bárdos, O. Horváth, É. Makó, M. Jakab, B. Zsirka, Coumarin-based quantification of hydroxyl radicals and other reactive species generated on excited nitrogen-doped TiO_2, J. Photochem. Photobiol. Chem. 404 (2021), https://doi.org/10.1016/j.jphotochem.2020.112913.
[59] K. Wang, Z. Bielan, M. Endo-Kimura, M. Janczarek, D. Zhang, D. Kowalski, A. Zielińska-Jurek, A. Markowska-Szczupak, B. Ohtani, E. Kowalska, On the mechanism of photocatalytic reactions on CuxO@TiO_2 core-shell photocatalysts, J. Mater. Chem. A 9 (2021) 10135–10145, https://doi.org/10.1039/d0ta12472a.
[60] M. Castañeda-Juárez, V. Martínez-Miranda, P.T. Almazán-Sánchez, I. Linares-Hernández, F. Santoyo-Tepole, G. Vázquez-Mejía, Synthesis of TiO_2 catalysts doped with Cu, Fe, and Fe/Cu supported on clinoptilolite zeolite by an electrochemical-thermal method for the degradation of diclofenac by heterogeneous photocatalysis, J. Photochem. Photobiol. Chem. 380 (2019) 111834, https://doi.org/10.1016/j.jphotochem.2019.04.045.
[61] M.R. Espino-Estévez, C. Fernández-Rodríguez, O.M. González-Díaz, J. Araña, J. P. Espinós, J.A. Ortega-Méndez, J.M. Doña-Rodríguez, Effect of TiO_2–Pd and TiO_2–Ag on the photocatalytic oxidation of diclofenac, isoproturon and phenol, Chem. Eng. J. 298 (2016) 82–95, https://doi.org/10.1016/j.cej.2016.04.016.
[62] A. Rey, E. Mena, A.M. Chávez, F.J. Beltrán, F. Medina, Influence of structural properties on the activity of WO_3 catalysts for visible light photocatalytic ozonation, Chem. Eng. Sci. 126 (2015) 80–90, https://doi.org/10.1016/j.ces.2014.12.016.
[63] A. Achilleos, E. Hapeshi, N.P. Xekoukoulotakis, D. Mantzavinos, D. Fatta-Kassinos, Factors affecting diclofenac decomposition in water by UV-A/TiO_2 photocatalysis, Chem. Eng. J. 161 (2010) 53–59, https://doi.org/10.1016/j.cej.2010.04.020.
[64] S.V. De Medeiros Lima, A.H. Da Silva Júnior, M.B. Quadri, A. Da Silva, Exploring a perovskite-type catalyst for diclofenac photodegradation: a comparative investigation with TiO_2, Water Air. Soil Pollut. 235 (2024) 700, https://doi.org/10.1007/s11270-024-07508-4.
[65] M.B.M. Roshtkhari, M.H. Entezari, Graphite/carbon-doped TiO_2 nanocomposite synthesized by ultrasound for the degradation of diclofenac, Environ. Sci. Pollut. Res. 31 (2024) 15105–15125, https://doi.org/10.1007/s11356-024-32182-8.
[66] D. Fabbri, M.J. López-Muñoz, A. Daniele, C. Medana, C. Paola, Photocatalytic abatement of emerging pollutants in pure water and wastewater effluent by TiO_2 and Ce-ZnO: degradation kinetics and assessment of transformation products, Photochem. Photobiol. Sci. 18 (2019) 845–852, https://doi.org/10.1039/c8pp00311d.
[67] C. Martínez, M.L. Canle, M.I. Fernández, J.A. Santaballa, J. Faria, Aqueous degradation of diclofenac by heterogeneous photocatalysis using nanostructured materials, Appl. Catal. B Environ. 107 (2011) 110–118, https://doi.org/10.1016/j.apcatb.2011.07.003.
[68] E. Mugunthan, M.B. Saidutta, P.E. Jagadeeshbabu, Photocatalytic activity of ZnO-WO_3 for diclofenac degradation under visible light irradiation, J. Photochem. Photobiol. Chem. 383 (2019) 111993, https://doi.org/10.1016/j.jphotochem.2019.111993.
[69] E. Valadez-Renteria, J. Oliva, K.P. Padmasree, V. Rodriguez-Gonzalez, Enhancing the removal of the diclofenac contaminant and accelerating the desalinization of seawater by using a biodegradable fibrous support functionalized with $Sr_{2.7}Ln_{0.3}Fe_{1.4}Co_{0.6}O_{7-\delta}$ (Ln = La or Nd) perovskites, Chem. Eng. J. 460 (2023) 141763, https://doi.org/10.1016/j.cej.2023.141763.
[70] M. Asadinamin, A. Živković, N.H. de Leeuw, S.P. Lewis, Role of interfacial morphology in Cu_2O/TiO_2 and band bending: insights from density functional theory, ACS Appl. Mater. Interfaces 16 (2024) 35781–35792, https://doi.org/10.1021/acsami.4c06081.
[71] Y. Yang, D. Xu, Q. Wu, P. Diao, Cu_2O/CuO bilayered composite as a high-efficiency photocathode for photoelectrochemical hydrogen evolution reaction, Sci. Rep. 6 (2016) 35158, https://doi.org/10.1038/srep35158.
[72] A. Kubiak, Z. Bielan, M. Kubacka, E. Gabała, A. Zgoła-Grześkowiak, M. Janczarek, M. Zalas, A. Zielińska-Jurek, K. Siwińska-Ciesielczyk, T. Jesionowski, Microwave-assisted synthesis of a TiO_2-CuO heterojunction with enhanced photocatalytic activity against tetracycline, Appl. Surf. Sci. 520 (2020) 146344, https://doi.org/10.1016/j.apsusc.2020.146344.
[73] W.C.J. Ho, Q. Tay, H. Qi, Z. Huang, J. Li, Z. Chen, Photocatalytic and adsorption performances of faceted cuprous oxide (Cu_2O) particles for the removal of methyl orange (MO) from aqueous media, Molecules 22 (2017) 677, https://doi.org/10.3390/molecules22040677.
[74] I.L.E. Gonzaga, C.C. Mercado, Copper ternary oxides as photocathodes for solar-driven CO_2 reduction, Rev. Adv. Mater. Sci. 61 (2022) 430–457, https://doi.org/10.1515/rams-2022-0043.
[75] D. Ghernaout, Advanced oxidation phenomena in electrocoagulation process: a myth or a reality? Desalination Water Treat. 51 (2013) 7536–7554, https://doi.org/10.1080/19443994.2013.792520.
[76] E.M. Cuerda-Correa, M.F. Alexandre-Franco, C. Fernández-González, Advanced oxidation processes for the removal of antibiotics from water. An overview, Water 12 (2020) 102, https://doi.org/10.3390/w12010102.
[77] M. Kowalkińska, A. Maximenko, A. Szkudlarek, K. Sikora, A. Zielińska-Jurek, Addressing challenges of $BiVO_4$ light-harvesting ability through vanadium precursor engineering and sub-nanoclusters deposition for peroxymonosulfate-assisted photocatalytic pharmaceuticals removal, Sep. Purif. Technol. 351 (2024) 127643, https://doi.org/10.1016/j.seppur.2024.127643.
[78] K. Shirai, G. Fazio, T. Sugimoto, D. Selli, L. Ferraro, K. Watanabe, M. Haruta, B. Ohtani, H. Kurata, C. Di Valentin, Y. Matsumoto, Water-assisted hole trapping at the highly curved surface of nano-TiO_2 photocatalyst, J. Am. Chem. Soc. 140 (2018) 1415–1422, https://doi.org/10.1021/jacs.7b11061.
[79] X. Ma, Y. Dai, M. Guo, B. Huang, Relative photooxidation and photoreduction activities of the {100}, {101}, and {001} surfaces of anatase TiO_2, Langmuir 29 (2013) 13647–13654, https://doi.org/10.1021/la403351v.
[80] M. Setvin, U. Aschauer, J. Hulva, T. Simschitz, B. Daniel, M. Schmid, A. Selloni, U. Diebold, Following the reduction of oxygen on TiO_2 anatase (101) step by step, J. Am. Chem. Soc. 138 (2016) 9565–9571, https://doi.org/10.1021/jacs.6b04004.
[81] J.Y. Hwang, G. Moon, B. Kim, T. Tachikawa, T. Majima, S. Hong, K. Cho, W. Kim, W. Choi, Crystal phase-dependent generation of mobile OH radicals on TiO_2: revisiting the photocatalytic oxidation mechanism of anatase and rutile, Appl. Catal. B Environ. 286 (2021) 119905, https://doi.org/10.1016/j.apcatb.2021.119905.
[82] S. Dudziak, J. Karczewski, A. Ostrowski, G. Trykowski, K. Nikiforow, A. Zielińska-Jurek, Fine-tuning the photocatalytic activity of the anatase {1 0 1} facet through dopant-controlled reduction of the spontaneously present donor state density, ACS Mater. Au 4 (2024) 436–449, https://doi.org/10.1021/acsmaterialsau.4c00008.
[83] P.E. De Jongh, D. Vanmaekelbergh, J.J. Kelly, Cu_2O: a catalyst for the photochemical decomposition of water? Chem. Commun. (1999) 1069–1070, https://doi.org/10.1039/a901232j.
[84] M.E. Aguirre, R. Zhou, A.J. Eugene, M.I. Guzman, M.A. Grela, Cu_2O/TiO_2 heterostructures for CO_2 reduction through a direct Z-scheme: Protecting Cu_2O from photocorrosion, Appl. Catal. B Environ. 217 (2017) 485–493, https://doi.org/10.1016/j.apcatb.2017.05.058.

MOST WIEDZY Downloaded from mostwiedzy.pl

[85] R. Hengerer, L. Kavan, P. Krtil, M. Grätzel, Orientation dependence of charge-transfer processes on TiO_2 (Anatase) single crystals, J. Electrochem. Soc. 147 (2000) 1467–1472.
[86] L. Kavan, M. Grätzel, S.E. Gilbert, C. Klemenz, J. Scheel, Electrochemical and photoelectrochemical investigation of single-crystal anatase, J. Am. Chem. Socienty 118 (1996) 6716–6723.
[87] S. Dudziak, C. Gómez-Polo, J. Karczewski, K. Nikiforow, A. Zielińska-Jurek, Insight into (electro)magnetic interactions within facet-engineered $BaFe_{12}O_{19}/TiO_2$ magnetic photocatalysts, ACS Appl. Mater. Interfaces 15 (2023) 56511–56525, https://doi.org/10.1021/acsami.3c13380.

MOST WIEDZY Downloaded from mostwiedzy.pl